sciendo

Geologos 30, 3 (2024): 171–194
https://doi.org/10.14746/logos.2024.30.3.17

GEOLOGOS

Characteristics and mineralogy of sediments in the Hongsa lignite deposit, northwestern Laos

Thunyapat Sattraburut[1], Yupa Thasod[2*], Benjavun Ratanasthien[2], Sirasit Vongvassana[1]

[1]Faculty of Environment and Resource Studies, Mahidol University, Nakhon Pathom 73170, Thailand;
e-mails: thunyapat.sat@mahidol.ac.th, sirasit.von@mahidol.ac.th
[2]Department of Geological Sciences, Faculty of Science, Chiang Mai University, Chiang Mai 50200, Thailand;
e-mails: yupa.t@cmu.ac.th, benjavun.r@cmu.ac.th
*corresponding author, e-mail: yupa.t@cmu.ac.th

Abstract

Two sediment cores from the central part of the Hongsa lignite deposit in northwestern Lao PDR (Lao People's Democratic Republic; Laos) have been analysed in order to understand their sedimentary characteristics using grain-size analysis, petrography, X-ray diffraction and scanning electron microscopy. This analysis has revealed that the deposit is primarily composed of fine-grained sediments, mainly silt and clay, with quartz as the dominant mineral and trace amounts of other minerals such as kaolinite, illite and montmorillonite. Gypsum and chlorite have also been found in some layers. Scanning electron microscope analysis has revealed a card-house structure of clay minerals, suggesting sedimentation from suspension driven by physico-chemical reactions influenced by pH and water chemistry. This arrangement increases porosity and water retention, significantly affecting the permeability and mechanical properties of sediments. Petrographic analysis has documented angular quartz and poorly sorted sediments, indicating minimal sediment reworking or short-distance sources. The palaeoenvironment of the Hongsa Basin, reconstructed from various rock units, suggests low-energy water conditions for the Underburden and moderate sediment supply in a wet forest swamp or bush moor environment for the Lower Lignite Zone Formation. The Middle Lignite Zone Formation indicates a more limited sediment supply in a similar environment, while Interburden Formation 1 suggests overbank deposits or stagnant water deposits. In summary, the Neogene Hongsa lignite deposit is characterised by fine-grained sediments, indicating low-energy water currents in mire environments. Occasional flood events brought coarser grains, although movement of facies should also be taken into account. The mineral composition suggests the presence of components derived from recycled sedimentary rocks along the northern border of the Hongsa Basin.

Keywords: grain size, petrography, X-ray diffraction, scanning electron microscopy, clay minerals, palaeoenvironment

1. Introduction

The Hongsa lignite deposit is located in the northwestern part of the Lao People's Democratic Republic (Lao PDR; Laos) and is considered to rank amongst the more important energy resources in Laos. More than 400 million tonnes (mill. Mg) of lignite are reserved for the Hongsa Mine-Mouth Thermal Power Plant, and approximately 370 mill. Mg are planned to be mined (Hongsa Power, 2024). Lignite is fed to three thermal power plants with a total capacity of 1,878 MW, which requires about 14.3 mill. Mg of lignite each year (Phusuwan et al., 2015). The reserve of the Hongsa open-pit mine is projected to last for 26 years of operations (Hongsa Power, 2024). Moreover, the Hongsa Power Plant generates large lignite consumption, which is expected to increase by 1.9% between 2018 and 2050, indicating a growing demand for lignite mining (Phouthonesy, 2021).

In order to understand the longevity and sustainability of the mining efforts, it is crucial to ex-

© 2024 Sattraburut T., Thasod Y., Ratanasthien B. & Vongvassana S. This is an open access article licensed under the Creative Commons Attribution-NonCommercial-NoDerivs License (http://creativecommons.org/licenses/by-nc-nd/4.0/).

amine the composition and geological history of the sediments in the Hongsa lignite deposit. The lignite-bearing complex consists of nine subunits, or seams, labelled A to I. They are divided into numerous thinner seams, reflecting the geological complexity of the region (Hofmann et al., 2008). These subunits include the following three main rock units: the Lower Lignite Zone Formation, the Middle Lignite Zone Formation and the Upper Lignite Zone Formation.

Palynological studies have indicated that deposition in this basin occurred between approximately 35 and 2 million years ago (Morley & Racey, 2011), while Vilaihongs & Areesiri (1997) suggested lignite deposition during the Neogene. Recent research by Sattraburut et al. (2021a, 2023) has dated Hongsa lignite deposit as Middle to Late Miocene, supported by palynological and fossil spore studies. Furthermore, petrographic analyses have revealed that the lignite formed in a mire (wet forest swamp and bush moor) environment, as indicated by the maceral contents, providing further insight into the depositional environment of these valuable lignite reserves (Sattraburut et al., 2017, 2021b).

Swelling clays are present in some areas of a section of the mine pit wall near the lignite seams, bottom conveyors and crushers. Serious mine safety and transport problems can occur when these swelling clays absorb water, especially during the rainy season. Therefore, thorough study of the sediments in the Hongsa lignite deposit is needed in order to avoid and prevent the above-mentioned problems.

Moreover, the origin of silica as a mineral matter in lignite is still unclear (Sattraburut, 2021b). This re-precipitated silica, especially in the form of thin hard bands, is one of the main problems in mine-mouth power plant processes as silica abrasion leads to boiler tube deterioration. High concentrations or large grain sizes of hard minerals such as quartz can also be a costly problem for mining and milling equipment due to abrasion.

Hofmann et al. (2008) recorded the mineral composition by using X-ray diffraction of soil samples from the surface of the main pit of the Hongsa Coal Mine. They showed that the predominant mineral was quartz (SiO_2), while minor minerals included kaolinite ($Al_2Si_2O_5(OH)_4$), illite ($KAl_2Si_3AlO_{10}(OH)_2$) and bayerite ($Al(OH)_3$). However, the samples were measured using an X-ray diffractometer at 5–80° 2θ with a scan rate of 0.02° 2θ per second at room temperature. This means that some minor minerals with concentrations of less than 5% or with d-spacings below 5° 2θ were not detected.

Therefore, the main purpose of the present study is to characterise the sediments in the Hongsa lignite deposit. The study of the sediments, especially the clay minerals, will lead to an interpretation of the source of these sediments, the genesis of the clays and the palaeoenvironment represented by the Hongsa lignite deposit. The results of the clay study will allow for an estimation of clay behaviour, which will be valuable for geotechnical considerations in mining operations and for future studies on mining processes and thermal power plant applications.

2. Study area and geological setting

2.1. Study area

The Hongsa lignite deposit is located in the northwestern region of Lao PDR, near the town of Hongsa in the province of Xayabouly. It is situated near the Thailand–Lao PDR border at the village of Huai Kon, Chaloem Prakiat District, Nan Province, and Muang Nguen, Xayabouly Province, Lao PDR. The Hongsa Basin has a roughly triangular and subelongated shape, extending in an ENE–WSW direction with a long axis of about 12 km and an average short axis of about 5 km (Fig. 1). Its geographical co-ordinates are between latitudes 19°39′N and 19°43′N and longitudes 101°14′E and 101°24′E. The concession area covers approximately 60 km^2 (Hofmann et al., 2008).

The Hongsa Basin is geographically defined by three distinct elevation levels: floodplains, hills and mountains. The higher elevations of the mountainous terrain are predominantly composed of Mesozoic red rocks. The peaks of the surrounding mountains range from 780 to 1,024 m a.s.l. Rolling hills are concentrated in the northern part of the basin. The elevation within the Hongsa Basin is approximately 351–400 m a.s.l. (Fig. 1). Terrain data were obtained from the ASTER Global Digital Elevation Model Version 3 (ASTER GDEM V3), available at https://gdemdl.aster.jspacesystems.or.jp/ (NASA/METI/AIST/Japan Spacesystems, and U.S./Japan ASTER Science Team, 2018).

2.2. Geological setting

The Hongsa Basin formed during the Cenozoic during tectonic movements across southeast Asia (Tapponier et al., 1986; Lacassin et al., 1997; Hall & Morley, 2004; Chaodumrong & Songtham, 2014; Jain, 2014; Friederich et al., 2016). Lao PDR is located in Sundaland, as are Vietnam, Cambodia, east-

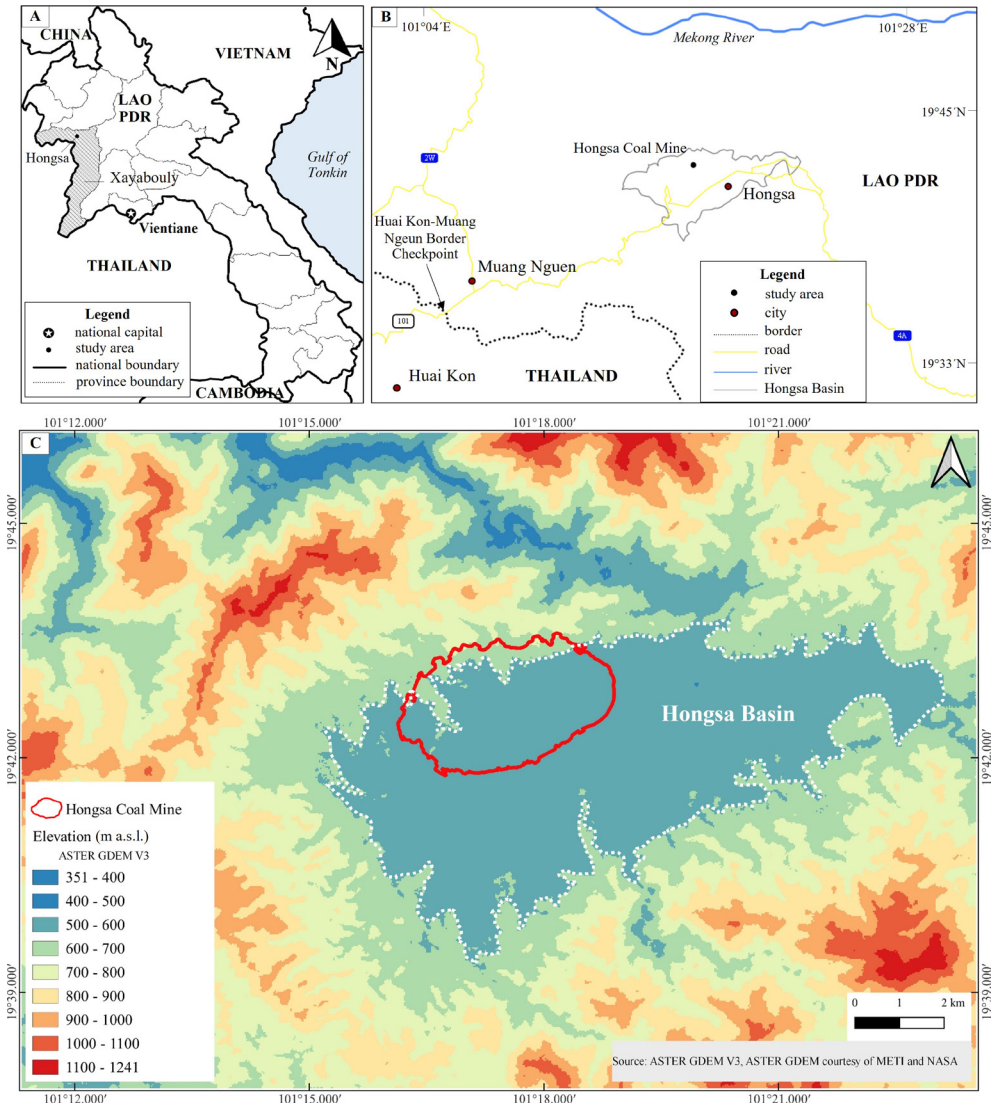

Fig. 1. Study area. **A, B –** Location of the Hongsa Basin; **C –** Elevation of the Hongsa Basin and adjacent area. The white dashed line indicates the approximate border of the Hongsa Basin.

ern Myanmar, Thailand, peninsular Malaysia, part of the islands of Borneo and Java and the island of Sumatra (Hall & Morley, 2004). This region is typically referred to as the continental core of southeast Asia, formed by the collision of the Indian plate and the Eurasian plate around 45 Ma, during the Middle Eocene (Friederich et al., 2016). However, Aitchison et al. (2007) suggested that this collision began around 34 Ma, near the Eocene–Oligocene boundary.

In southeast Asia, many basins exhibit a half-graben geometry due to tensional stress that was dominant during the Eocene–Oligocene (Hall & Morley, 2004). Burri (1989) reported that strike-slip movements were common in the basins, resulting in extensional faulting and very complex, highly faulted basin margins. Around 20 Ma (during the Miocene), in a compressional regime, mountain building and basin inversion began. This tectonic activity continued at least until the Pliocene (Hall & Morley, 2004). However, the geology of Laos and its tectonic setting is not well documented in detail. Most of the existing information is based on the interpretation of satellite imagery and basic geological maps.

Given this tectonic context, several sediment studies in Laos have focused primarily on the Mekong River Basin, with investigations dedicated to sediment transport dynamics, impacts of hydropower development and climate change effects. Research by Piman and Shrestha (2017) emphasised how infrastructure projects, particularly dam constructions, disrupt sediment delivery to downstream regions, raising concerns about sustaina-

ble sediment management. Additionally, studies assessing the implications of climate change have revealed that environmental stressors significantly alter sediment dynamics, with potential future impacts on sediment accumulation in the basin (Shrestha et al., 2018). These sedimentary investigations are particularly relevant in the light of geological studies related to the Hongsa lignite deposit. They provide insights into historical sedimentary and environmental processes through sedimentological and palynological analyses. Overall, these studies highlight the critical need for integrated sediment management in Laos amidst ongoing environmental changes. This will allow us to demonstrate the relationship between the complex geological history of the region and the contemporary sediment dynamics.

Within this context, a clear understanding of the geological framework of the Hongsa Basin is essential. The basement of the basin consists of Mesozoic sedimentary rocks. On the western and eastern sides of the basin, these are of late Mesozoic age (Fig. 2) and comprise predominantly fine-grained sandstone, prominent at lower levels. The uppermost part of this sequence consists of thick evaporates. Middle Mesozoic sedimentary rocks, mainly of Late Triassic to Early Cretaceous age, are situated on the southwestern side of the basin. They are primarily terrestrial sedimentary rocks, mainly sandstone, similar to the formations on the other sides of the basin (Fig. 2).

Within the Hongsa Basin, Neogene strata comprise mainly light grey silty clays, which are the host lignite deposits. Some layers also contain hard beds and siltstones (Fig. 2). Their total thickness exceeds 100 m. These beds are inclined towards the Hongsa Coal Mine (Hofmann et al., 2008). The coals found here are of low rank, hence they are classified as lignites, i.e., lignite A and lignite B. They were laid down mainly in a mire environment with a high mineral content (Sattraburut et al., 2017, 2021b). The uppermost layer consists of Quaternary sediments (Fig. 2), including alluvial clay, silt, sand and gravel derived from the Mekong River and its tributaries.

The stratigraphy of the Hongsa lignite deposit is similar to that of the entire Hongsa Basin. A total of ten rock units have been differentiated; from bottom to top (Fig. 3): Basement Rock, Underburden Formation 1 and 2, Lower Lignite Zone Formation, Interburden Formation 2, Middle Lignite Zone Formation, Interburden Formation 1, Upper Lignite Zone Formation, Overburden and Quaternary deposits (Hofmann et al., 2008). The lignite seams within the Hongsa Coal Mine are categorised into nine subunits, labelled A to I. However, the presence of inorganic sediments between and within these lignite seams (layers, subunits) is visible (Fig. 3). Thus, these multiple lignite layers pose a challenge as far as their correlation across the Hongsa Basin is concerned.

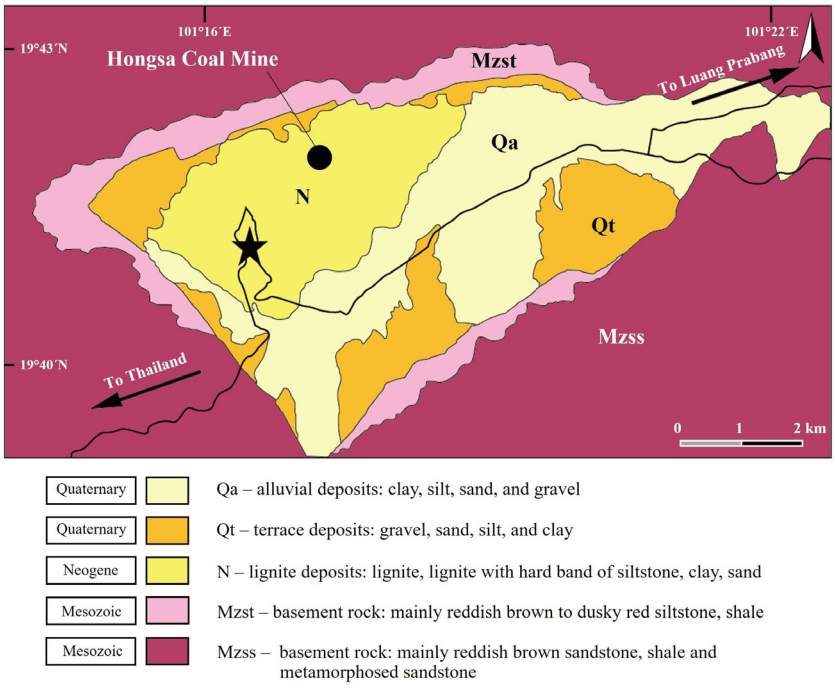

Fig. 2. Geological map of the Hongsa Basin (modified from Hofmann et al., 2008). The black star indicates the location of the Hongsa Mine-Mouth Power Plant.

3. Methodology

3.1. Sampling

Samples examined for the present paper were collected from boreholes A and B, located near the central part of the Hongsa Coal Mine (Fig. 4) and approximately 1 km apart. Borehole A reached a depth of 331.4, borehole B a depth of 212.0 m. The cores were split lengthwise, and one-half was collected in plastic bags. Sampling intervals varied according to sediment size and colour, averaging 2–5 m for borehole A and 1 m for borehole B. Details of the sampling locations of both boreholes are shown in Figure 4. As a result of extensive faulting within the basin, borehole B was found to penetrate the Upper Lignite Zone Formation, with no presence of the Overburden. This absence may likely be attributed to fault displacement or erosion associated with tectonic activity. Due to the composition of the Middle and Lower Lignite Zone formations, inorganic samples were rare. Twenty-one samples were collected from borehole A and twenty from borehole B. These samples, comprising generally light to medium grey, unconsolidated silt and clay (Tables 1, 2), were photographed, described and analysed for grain size. The mineralogy of the sediments was analysed using petrography, X-ray diffraction and scanning electron microscopy.

3.2. Grain-size analysis of sediments

This analysis aims to determine the relative proportions of different grain sizes in sediment samples using sieving and hydrometer methods. Sediments from borehole B of the Hongsa lignite deposit were dried, wet-sieved on 200-mesh sieves, and then dry-sieved for 15 minutes. The hydrometer method, according to ASTM D 422−63 standards (ASTM International, 2008), was employed to analyse the fine grain sizes. Data from both methods were plotted on a semi-logarithmic graph of grain diameter *vs* percent finer. In addition, the moment method was applied for statistical grain-size analysis, offering detailed insights into sediment transport and depositional environments. This method calculates grain-size distribution parameters using statistical moments (mean, sorting, skewness and kurtosis) derived from the cumulative frequency curve of the grain-size data (Folk & Ward, 1957; Blott & Pye, 2001).

Table 1. Description and thickness of sediment samples collected from borehole A in the Hongsa lignite deposit. For sample locations, see Figures 3 and 4. Abbreviations: Overburden (OB), sediment parting within seam H and above, Underburden (UB).

Sample no.	Lignite seam	Description	Thickness (m)
01	OB	Clay, yellowish brown to light red, hard, semi-consolidated, loose	2.30
05	OB	Silty clay and clay, light yellowish grey to medium grey, hard, semi-consolidated, loose	8.45
07	OB	Clay and silty clay, light grey to medium light grey, hard	3.70
10	I3	Clay and silty clay, very light grey to light grey, hard	4.50
12	I3	Clay and silty clay, light grey, hard, semi-consolidated, loose	4.30
16	I3	Clay, light grey to medium light grey, hard	2.85
20	I2	Clay, light yellowish grey, hard	0.40
26	I2	Sandy clay, yellowish grey, hard	1.90
29	I2	Silty clay, light grey, hard, semi-consolidated, organic fragments, loose	5.95
31	I1	Carbonaceous clay, medium grey, hard, organic fragments, semi-consolidated, loose	0.65
38	s(HI)	Silty clay, very light grey to light grey, hard	2.80
43	s(HI)	Carbonaceous clay, yellowish grey to medium grey, hard, organic fragments	2.00
50	s(HI)	Silty clay, light grey to brownish-grey, hard, semi-consolidated	5.60
56	s(HI)	Clay and sandy clay, light grey to medium light grey, hard	3.10
59	H3	Clay and silty clay, light grey to medium light grey, hard	4.60
66	H2	Clay, very light grey to light grey, hard	0.70
70	H2	Clay and carbonaceous clay, light grey to medium grey, hard	0.20
80	G1	Carbonaceous clay, medium grey to medium dark grey, hard, organic fragments	2.55
89	C5	Clay, brownish grey to medium grey	0.55
97	UB	Clay, light grey, hard	2.70
99	UB	Silty clay, light grey to medium grey, hard	4.20

Table 2. Description and thickness of sediment samples collected from borehole B in the Hongsa lignite deposit. For sample locations, see Figures 3 and 4.
Abbreviation: Interburden Formation 1 (IF1), Underburden (UB).

Sample no.	Lignite seam	Description	Thickness (m)
HS01	H3	Clay, medium grey, hard semi-consolidated, loose	2.00
HS02	H3	Clay and silty clay, light grey to brownish grey, hard	2.50
HS03	H3	Clay and carbonaceous clay, medium light grey to brownish grey, hard	1.50
HS06	G3	Clay and carbonaceous clay, brownish grey to dusky brown, hard, semi-consolidated, loose	12.25
HS07	G2	Silty clay and clay, light grey to medium grey, stiff, semi-consolidated with some pale yellowish orange siltstone hard band, some laminated organic layered	1.40
HS10	G2	Clay, medium grey, hard, graded to brownish grey clay with some laminated organic layered	1.50
HS11	IF1	Clay, brownish grey, hard, loose	0.65
HS12	IF1	Silty clay, light grey, hard	1.90
HS13	IF1	Clayey sand, light grey, stiff, semi-consolidated sediments, with some medium to coarse sand, loose	0.75
HS14	IF1	Clay, brownish grey, hard	2.50
HS15	IF1	Silty clay, light grey, hard	2.05
HS16	IF1	Silty clay, light grey, hard	1.30
HS18	IF1	Clay and clayey sand, light grey to brownish grey, stiff, semi-consolidated sediment, with some medium to coarse sand, loose	2.90
HS19	IF1	Clayey sand and sand, stiff, semi-consolidated sediments, loose	4.05
HS20	IF1	Silty clay, light grey, hard	2.00
HS21	IF1	Clayey sand, medium grey, hard	3.90
HS22	IF1	Clay, medium grey, hard	2.30
HS23	IF1	Silty clay, medium grey, hard	1.30
HS24	IF1	Clay and carbonaceous clay, medium grey to medium dark grey, hard	3.45
HS26	UB	Clay, medium grey, hard	0.50

Table 3. Percentage of sediment size classes from borehole B. For sample locations, see Figures 3 and 4. Abbreviations: parting in seam H (H), parting in seam G (G), Interburden Formation 1 (IF1), Underburden (UB)

Sample	Rock unit	Size class				Nomenclature (after Folk, 1980)
		gravel	sand	silt	clay	
HS01	H	–	5.58	44.42	50.00	mud
HS02	H	–	7.43	52.57	40.00	mud
HS03	H	–	28.91	46.09	25.00	sandy mud
HS06	G	0.45	21.11	43.44	35.00	slightly gravelly muddy sand
HS07	G	–	11.93	50.07	38.00	sandy mud
HS10	G	–	12.70	52.30	35.00	sandy mud
HS11	IF1	–	8.43	44.57	47.00	mud
HS12	IF1	–	4.28	56.72	39.00	mud
HS13	IF1	–	5.77	57.23	37.00	mud
HS14	IF1	3.95	37.38	36.67	22.00	slightly gravelly muddy sand
HS15	IF1	–	8.14	59.86	32.00	mud
HS16	IF1	0.27	18.97	52.76	28.00	slightly gravelly muddy sand
HS18	IF1	2.20	11.39	54.41	32.00	slightly gravelly muddy sand
HS19	IF1	–	18.52	44.48	37.00	sandy mud
HS20	IF1	–	13.46	54.54	32.00	sandy mud
HS21	IF1	–	7.77	61.23	31.00	mud
HS22	IF1	1.38	29.83	38.79	30.00	slightly gravelly muddy sand
HS23	IF1	–	3.57	51.43	45.00	mud
HS24	IF1	–	12.58	52.42	35.00	sandy mud
HS26	UB	–	26.41	16.59	57.00	sandy mud

Table 4. Weight percent of sediments in φ scale. For sample locations, see Figures 3 and 4.

Sample	Class (Φ)													
	–3 – –2	–2 – –1	–1 – 0	0 – 1	1 – 2	2 – 3	3 – 4	4 – 5	5 – 6	6 – 7	7 – 8	8 – 9	9 – 10	> 10
HS01	0.00	0.16	0.67	0.33	0.60	1.87	2.36	2.17	8.20	5.99	3.11	7.76	8.03	58.75
HS02	0.00	0.35	0.40	0.20	0.38	2.67	5.57	6.45	8.37	0.72	12.10	0.98	11.97	49.84
HS03	0.00	2.21	11.42	5.71	5.45	3.04	4.12	9.17	6.21	5.26	6.45	2.79	5.79	32.38
HS06	0.51	0.16	0.41	0.20	0.45	4.68	9.38	8.89	7.95	6.73	8.25	3.58	7.40	41.41
HS07	0.00	0.51	0.16	0.08	0.85	5.36	6.20	6.19	14.73	7.52	6.93	4.57	8.88	38.02
HS10	0.00	0.13	0.28	0.14	0.39	4.63	10.46	10.06	11.56	8.41	9.07	2.47	8.21	34.19
HS11	0.00	1.54	2.46	1.23	1.23	1.27	3.34	6.35	0.66	0.00	1.79	3.81	7.71	68.61
HS12	0.00	0.21	0.30	0.15	0.38	1.47	2.18	3.30	10.09	17.23	0.00	10.15	7.44	47.10
HS13	0.00	0.27	0.77	0.38	0.50	1.59	4.76	6.50	6.31	4.50	11.31	5.48	9.02	48.61
HS14	4.71	2.02	3.43	1.72	3.80	14.10	12.90	5.88	9.81	4.67	6.17	1.63	3.35	25.81
HS15	0.00	0.59	0.52	0.26	0.38	2.58	5.78	9.34	13.57	14.95	8.64	3.74	3.37	36.28
HS16	0.28	0.03	0.25	0.13	0.69	8.36	11.84	8.98	13.51	11.47	0.00	5.49	8.00	30.97
HS18	2.38	0.46	0.52	0.26	0.69	4.37	5.45	2.72	10.91	8.79	12.07	3.54	11.75	36.09
HS19	0.00	0.03	0.22	0.11	0.36	7.11	14.41	11.79	13.44	6.43	7.41	1.43	5.60	31.66
HS20	0.00	0.76	1.71	0.86	0.94	3.76	7.72	7.17	10.97	8.35	6.38	4.18	11.54	35.66
HS21	0.00	0.37	0.58	0.29	0.75	2.42	3.81	3.27	11.80	14.87	5.69	8.94	13.42	33.79
HS22	1.63	0.65	1.41	0.70	5.47	15.24	7.70	1.49	5.23	5.21	3.48	6.81	4.24	40.74
HS23	0.00	0.15	0.67	0.33	0.61	1.08	2.86	5.46	4.43	7.20	3.05	16.10	4.84	53.22
HS24	0.00	0.13	0.62	0.31	0.65	4.99	7.74	5.55	10.54	4.86	11.36	5.65	7.52	40.08
HS26	0.00	10.62	5.31	2.65	3.82	2.78	1.87	1.71	2.04	2.78	1.27	1.83	2.49	60.83

The size classes of gravel, sand, silt and clay were calculated using sieve and hydrometer analysis in terms of weight percent for each class. The grain-size results are presented in Tables 3 and 4. Cumulative curves were plotted on the probability percent scale of 20 sediment samples from borehole B. Various statistical parameters of grain size were obtained from these curves. The median, graphical mean, standard deviation, skewness and graphical kurtosis are presented in Table 5.

3.3. Petrography of sedimentary rocks

In the study area unconsolidated sediments predominate, and there are not many sedimentary rocks. As a result, there are not enough samples to consider grain-size variations throughout the samples from both boreholes. Rocks were found only in the Interburden Formation 1 from borehole B, the parting within the seam H from borehole A and within the seam G from borehole B. All of them are located in the Upper Lignite Zone Formation (Fig. 4). Six sedimentary rock samples were thin sectioned for petrographic examination under a light microscope. Fresh, cleaned samples were selected for thin sectioning.

3.4. X-ray diffraction

Twenty-one samples from borehole A and twenty from borehole B were analysed to determine the bulk chemical composition of the sediments using the X-ray diffraction method (XRD). Samples were oven-dried at 40°C overnight and ground to powder before being analysed on a Bruker X-ray diffractometer (model D8 Advance) at 2–60° 2θ. In addition, two sets of samples were oriented and treated with ethylene glycol. The d-spacings obtained from the first diffractogram were then compared with the d-spacings of standard minerals as recorded by the American Society for Testing and Materials (ASTM).

Semi-quantitative estimations of mineral proportions were made by selecting the highest intensity of the d-spacing reflection for each mineral. The mineral composition was calculated on the basis of

the half peak area, determined by multiplying the peak height by the half width at half maximum. This method mitigates issues related to baseline inclines and peak overlaps (Ratanasthien, 1975). The total calculated area was normalised to 100 per cent, and mineral proportions were expressed as percentage values. While this approach may result in slight over- or underestimations, comparisons are most accurate when samples contain similar constituents (Ratanasthien, 1975; Thasod et al., 2007).

3.5. Scanning electron microscopy

In order to study external textures and mineral composition under a scanning electron microscope (SEM), a piece of inorganic sediment (approximately 0.5 × 0.5 × 0.5 cm) was mounted on a metal stub using adhesive carbon tape. The sample was then coated with a layer of gold approximately 40–60 nm thick to enhance conductivity and prevent charging during observation. This gold coating is critical, as it ensures that secondary electrons can be emitted from the surface of the sample, providing detailed topographic images. Once prepared, the sample is observed under the SEM, which allows for high-resolution imaging of the mineral surfaces. In conjunction with the SEM, an Energy Dispersive X-ray Spectrometer (EDS) was utilised to analyse the elemental composition of the minerals. The EDS system detects characteristic X-rays emitted from the sample when this is bombarded with an electron beam. This technique provides qualitative and quantitative information on the elements present in the sample, allowing for accurate identification of mineral compositions. The experiments were carried out at the Central Science Laboratory, Faculty of Science, Chiang Mai University.

4. Results

4.1. Grain-size distribution

Our results show that the median size ranges from 4.13 to 9.40 with an average of 7.47 on the φ scale. The mean size ranges from 4.85 to 7.99 with an average of 6.73 on the φ scale (Table 5), indicating that the sediments are mostly fine according to Wentworth's size class and show a predominance of medium to fine silt. The φ standard deviation of the samples ranges from 2.24φ to 4.26φ with an average of 2.93φ (Table 5), which is interpreted as very poorly sorted. This distribution shows a rather low degree of heterogeneity, due to the location of the supply sources, transport processes and environmental energy (Kumar & Patterson, 2008). The skewness ranges from -0.89 to 0.15 with an average of -0.39, indicating that the samples are highly skewed to slightly skewed, with most being highly skewed. The kurtosis values range from 0.53 to 2.14 with an average of 0.77 (Table 5), indicating that the samples are very platykurtic to very leptokurtic, with the majority being platykurtic.

In the present study, our interpretation of the depositional history of the siliciclastic sediments focused on three rock units: Underburden, Interburden Formation 1 and Upper Lignite Zone For-

Table 5. Grain-size parameters calculated by the method of moments. For sample locations, see Figures 3 and 4. Abbreviations: parting in seam H (H), parting in seam G (G), Interburden Formation 1 (IF1), median (φ) (Med), graphic mean (φ) (Mean), inclusive graphic standard deviation (SD), inclusive graphic skewness (Sk), graphic kurtosis (K_G).

Sample	Rock unit	Med	Mean	SD	Sk	K_G
HS01	H	9.20	7.98	2.32	–0.78	1.05
HS02	H	8.96	7.56	2.59	–0.74	0.80
HS03	H	5.53	4.85	4.26	–0.22	0.57
HS06	G	7.71	6.83	2.88	–0.43	0.61
HS07	G	7.31	6.81	2.75	–0.30	0.67
HS10	G	6.50	6.36	2.85	–0.10	0.60
HS11	IF1	9.40	7.68	2.74	–0.86	2.14
HS12	IF1	8.62	7.73	2.24	–0.59	0.69
HS13	IF1	8.90	7.61	2.51	–0.72	0.83
HS14	IF1	4.13	4.86	4.01	0.08	0.71
HS15	IF1	6.25	6.52	2.64	0.04	0.64
HS16	IF1	5.58	5.91	2.95	0.10	0.58
HS18	IF1	7.40	6.90	2.79	–0.33	0.78
HS19	IF1	5.45	5.90	2.94	0.15	0.56
HS20	IF1	7.35	6.65	2.96	–0.36	0.68
HS21	IF1	7.72	7.26	2.44	–0.35	0.75
HS22	IF1	7.28	6.16	3.52	–0.44	0.54
HS23	IF1	9.10	7.99	2.24	–0.74	1.01
HS24	IF1	7.65	6.87	2.80	–0.41	0.68
HS26	UB	9.29	6.07	4.19	–0.89	0.53
average		7.47	6.73	2.93	–0.39	0.77
minimum		4.13	4.85	2.24	–0.89	0.53
maximum		9.40	7.99	4.26	0.15	2.14

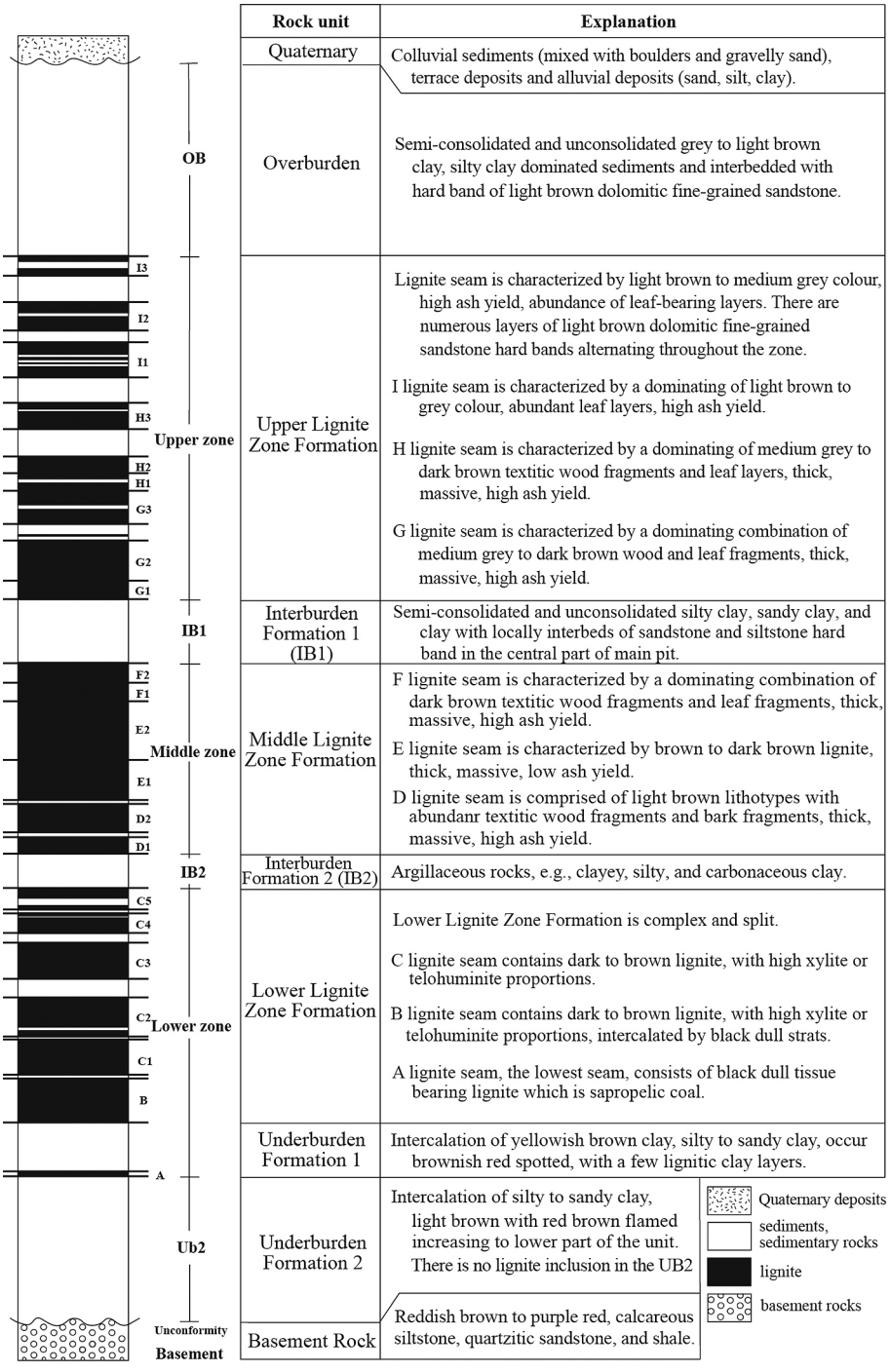

Fig. 3. General stratigraphy of the Hongsa lignite deposit (modified from Hofmann et al., 2008; Sattraburut et al., 2021b).

mation (see Figs. 3, 4). Tables 6 and 7 show the average weight percent of sediments on the φ scale and the average grain-size parameters calculated by the moment method based on rock units, respectively.

4.2. Petrography of sedimentary rocks

Most of the samples are mudstone, with the remainder being siltstone and sandstone. The main detrital component of the sandstone and siltstone is monocrystalline quartz. Some rock fragments were also observed; these typically were sedimentary lithic fragments. The matrix of the rocks generally consisted of quartz, and the cementing materials were silica and clay minerals (Figs 5, 6). According to the petrographic study, the textural maturity of the samples is immature and submature, containing more than 5 per cent of mud matrix. The grains are poorly sorted and subrounded to subangular. All

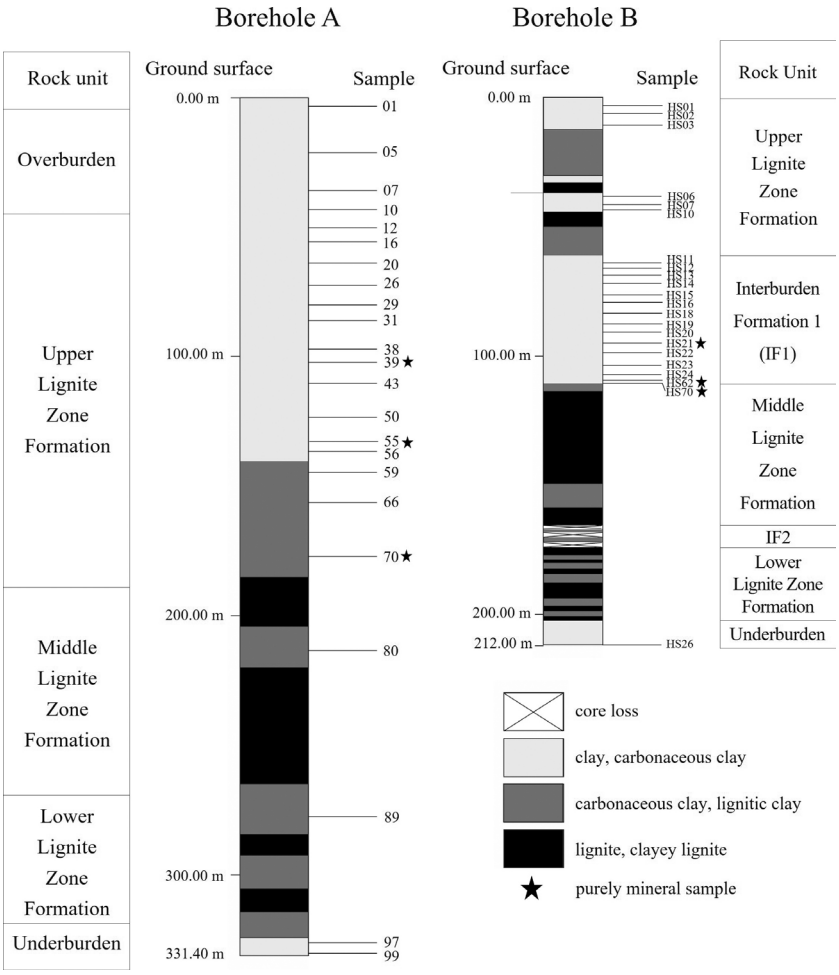

Fig. 4. Schematic lithostratigraphy of boreholes A and B with marked sampling locations for laboratory tests.

Table 6. Average weight percentage of sediments for rock units on the φ scale. Abbreviations: parting in seam H (H), parting in seam G (G), Interburden Formation 1 (IF1), Underburden (UB).

Rock Unit	Class (Φ)													
	–3 – –2	–2 – –1	–1 – 0	0 – 1	1 – 2	2 – 3	3 – 4	4 – 5	5 – 6	6 – 7	7 – 8	8 – 9	9 – 10	> 10
H	0.00	0.91	4.16	2.08	2.14	2.53	4.02	5.93	7.59	3.99	7.22	3.84	8.60	46.99
G	0.17	0.27	0.28	0.14	0.56	4.89	8.68	8.38	11.41	7.55	8.08	3.54	8.16	37.87
IF1	0.69	0.55	1.04	0.52	1.27	5.26	6.96	5.98	9.33	8.35	5.95	5.92	7.52	40.66
UB	0.00	10.62	5.31	2.65	3.82	2.78	1.87	1.71	2.04	2.78	1.27	1.83	2.49	60.83

Table 7. Average grain-size parameters for rock units calculated using the method of moments. Abbreviations: parting in seam H (H), parting in seam G (G), Interburden Formation 1 (IF1), Underburden (UB).

Rock unit	Med	Mean	SD	Sk	KG
H	7.90	6.80	3.06	–0.58	0.81
G	7.17	6.67	2.83	–0.28	0.63
IF1	7.29	6.77	2.83	–0.34	0.81
UB	9.29	6.07	4.19	–0.89	0.53

samples show a predominance of quartz grains of various sizes in the clay matrix (Figs 5, 6).

The study area is covered primarily by sediments, with only a limited presence of sedimentary rocks. Thus, the available samples are insufficient to assess grain-size variations through petrographic analysis thoroughly across the boreholes. It may be assumed that there were several periods of flooding that brought sediments from their sources to be deposited in the study area. For example, many sandstone or siltstone beds are found between thick layers of mudstone. The sandstone layers accumulated

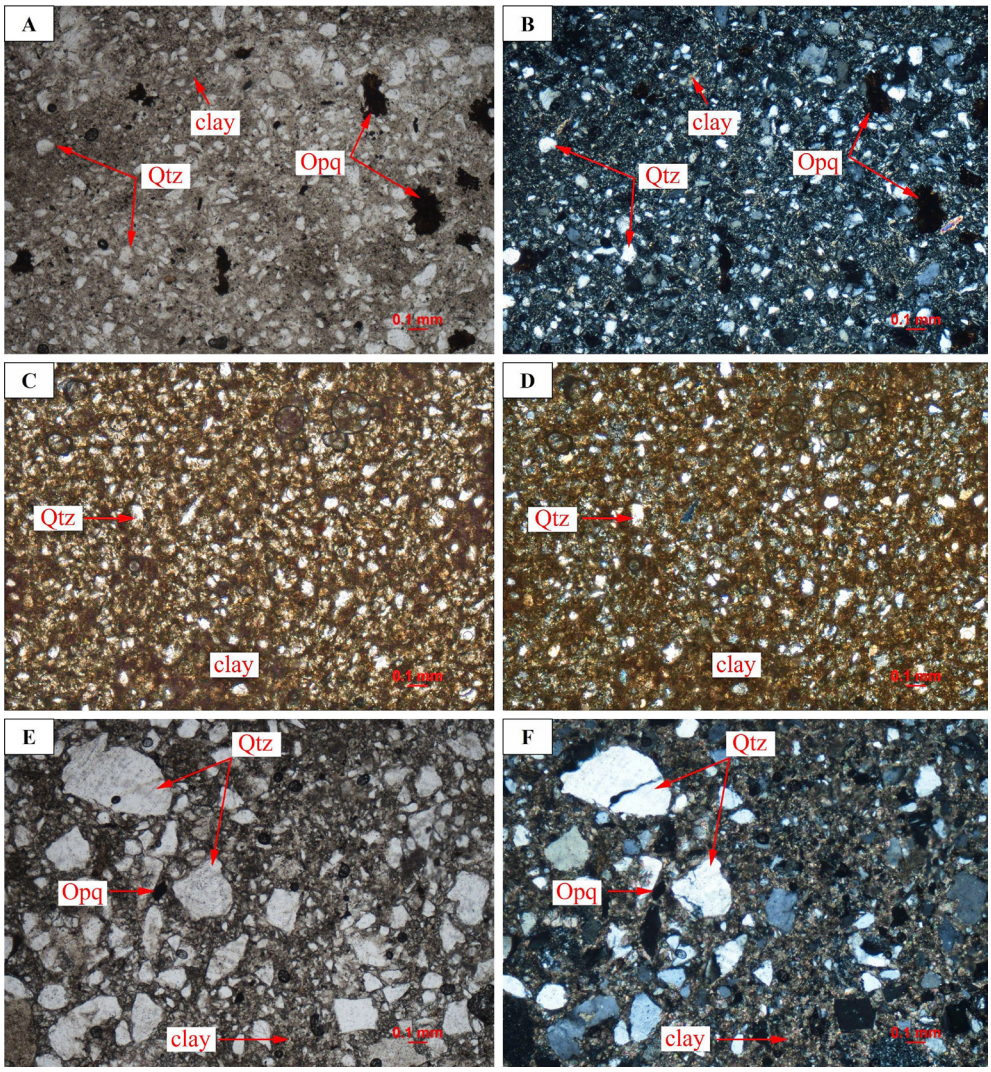

Fig. 5. Photomicrographs of sedimentary rocks from borehole A under plane-polarised light (A, C, E) and crossed-polarised light (B, D, F). **A, B –** Sandstone from sample 39 (seam H); **C, D –** Sandstone from sample 55 (seam H); **E, F –** Sandstone from sample 70 (seam H). Abbreviations: quartz – Qtz, opaque mineral – Opq, clay minerals – clay.

due to the supply of sediments during the flood. In addition, the sandstones tend to contain the same minerals with similar shapes, reflecting the close proximity of sources.

4.3. Mineral composition using X-ray diffraction

X-ray diffraction results indicate that the sediments formed by similar mineral associations in varying proportions. The major composition is quartz, with kaolinite, illite and montmorillonite as minor components. Gypsum and chlorite are present in small amounts in some samples from boreholes A and B, respectively (Tables 8, 9).

Overall, the samples from borehole A show a trend towards quartz, as opposed to kaolinite, illite and montmorillonite. Quartz ranges from 55 to 88 per cent (average of 74.10 per cent). Kaolinite and illite range from 5 to 18 per cent (average of 9.57 per cent) and 4 to 26 per cent (average of 10.57 per cent), respectively. Montmorillonite ranges from 2 to 10 per cent (average of 5.48 per cent). Gypsum is shown as a trace in samples 01, 05, 66, 80, 89, 97 and 99. Traces of chlorite were observed in samples 01 and 05. It is clear that all samples consist of a high amount of quartz (Tables 8, 9).

Similar to borehole A, samples from borehole B show a trend of quartz, as opposed to kaolinite, illite and montmorillonite. The samples consist of 62 to 93 per cent quartz (average of 80 per cent). Kaolinite ranges from 2 to 18 per cent (average of 7.6 per

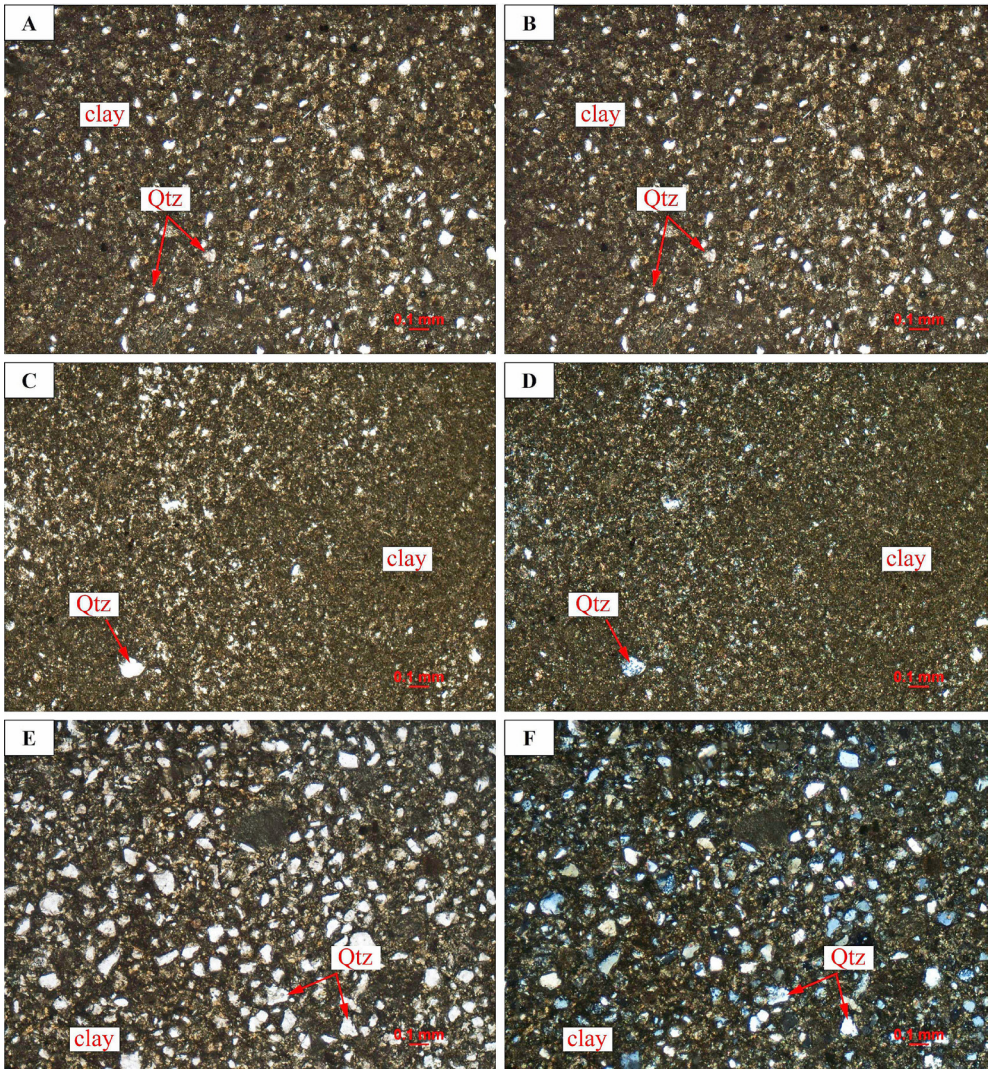

Fig. 6. Photomicrographs of sedimentary rocks from borehole A under plane-polarised light (A, C, E) and crossed-polarised light (B, D, F). **A, B –** Siltstone from sample HS21 (seam G); **C, D –** Mudstone from sample HS62 (IF1); **E, F –** Sandstone from sample HS70 (IF1). Abbreviations: quartz – Qtz, clay minerals – clay.

cent). Illite and montmorillonite range from 4 to 13 per cent (average of 7.65 per cent) and 1 to 9 per cent (average of 4.6 per cent), respectively (Tables 8, 9).

Moreover, the grain-size results are considered in relation to the mineral composition. In terms of grain size, inorganic sediments in the Hongsa Basin typically consist of fine to very fine grains, i.e., clays and silts as described below.

4.4. Scanning electron microscopy

Clay minerals from the Hongsa lignite deposit were observed under an SEM. The results show a predominance of illite (Figs. 7, 8), in the form of irregular, flaky clay platelets oriented in a card-house microfabric, reflecting the settling of particles from suspension. Such illite grains are found in each rock formation examined in the present study. The Energy Dispersive X-ray Spectrum (EDS) pattern from the point marked in Figure 8C reveals the main elements to be Si, Al and K, with a small amount of Fe (Fig. 9). The results of EDS, based on the chemical composition, suggests the presence of illite in the examined sediments.

Illite is the name given to the micaceous minerals present in the clay-size fraction of sedimentary rocks (Chamley, 1989). Differences in shape and arrangement are used to indicate the origin of illite (Welton, 2003), such as thin illitic clay rims (dust line), illite mat and flaky illite. In the SEM study, illite platelets tended to appear to be randomly arranged. Many platelets surrounded larger sediment grains in an onion-skin arrangement (Bennett et al.,

Table 8. Bulk composition of minerals in borehole A from the Hongsa lignite deposit (%). Abbreviations: Overburden (OB), Upper Lignite Zone Formation (UF), Lower Lignite Zone Formation (LF), Underburden (UB), quartz (Qtz), kaolinite (Kao), illite (Ill), montmorillonite (Mont), gypsum (Gyp) and chlorite (Chl).

Sample	Rock unit	Qtz	Kao	Ill	Mont	Gyp	Chl
01	OB	72	9	11	8	trace	trace
05	OB	62	6	26	6	trace	trace
07	OB	88	5	4	3	0	0
10	UF	69	13	13	5	0	0
12	UF	73	8	14	5	0	0
16	UF	74	9	8	5	4	0
20	UF	75	9	11	5	0	0
26	UF	74	9	9	8	0	0
29	UF	85	5	5	5	0	0
31	UF	64	18	11	7	0	0
38	UF	83	7	5	5	0	0
43	UF	72	12	7	9	0	0
50	UF	87	5	5	3	0	0
56	UF	81	8	8	3	0	0
59	UF	87	5	5	3	0	0
66	UF	75	9	12	4	trace	0
70	UF	84	7	7	2	0	0
80	UF	64	13	16	7	trace	0
89	LF	55	17	18	10	trace	0
97	UB	71	9	14	6	trace	0
99	UB	61	18	13	6	2	0

Table 9. Bulk composition of minerals in borehole B from the Hongsa lignite deposit (%). Abbreviations: Overburden (OB), Upper Lignite Zone Formation (UF), Lower Lignite Zone Formation (LF), Underburden (UB), quartz (Qtz), kaolinite (Kao), illite (Ill), montmorillonite (Mont), gypsum (Gyp) and chlorite (Chl).

Sample	Rock unit	Qtz	Kao	Ill	Mont	Gyp	Chl
HS01	UF	70	9	13	8	0	0
HS02	UF	79	8	8	5	0	0
HS03	UF	69	10	10	9	2	trace
HS06	UF	77	9	9	5	0	trace
HS07	UF	85	8	5	2	0	0
HS10	UF	73	10	11	6	0	trace
HS11	IF1	69	14	11	6	0	trace
HS12	IF1	74	10	8	8	0	0
HS13	IF1	83	6	5	6	0	0
HS14	IF1	88	4	4	4	0	0
HS15	IF1	89	3	4	4	0	0
HS16	IF1	91	3	4	2	0	0
HS18	IF1	89	4	5	2	0	0
HS19	IF1	93	2	4	1	0	0
HS20	IF1	85	5	7	3	0	0
HS21	IF1	79	9	10	2	0	0
HS22	IF1	88	5	5	2	0	0
HS23	IF1	80	7	8	5	0	0
HS24	IF1	77	8	9	6	0	0
HS26	UB	62	18	13	6	0	trace

1991). The random arrangement of small platelets is consistent with the broadening of the XRD peaks (compare Figs. 9 and 10). The small particle size of the material typically causes broadening in its diffraction peak (Virk, 2015).

4.5. Swelling clay

Swelling clays, particularly montmorillonite of the smectite group, are distinguished by their ability to expand significantly when hydrated. This expansion occurs as water molecules penetrate the interlayer spaces within the clay structure, leading to an increase in volume. To analyse these properties, XRD techniques are employed, often utilising glycolation to differentiate between swelling and non-swelling clays. For example, montmorillonite exhibits a shift in its diffraction pattern to lower angles after glycolation. This indicates its capacity for expansion, while non-swelling clays show no change (Brindley & Brown, 1980; Moore & Reynolds, 1997; Jackson, 2018).

Montmorillonite can swell to several times its dry volume; however, not all clays exhibit this behaviour upon hydration. In XRD analysis, samples were prepared as oriented and glycolated mounts, with scans performed on both untreated and glycolated samples. The low-angle diffraction data illustrated expansion of montmorillonite along the c-axis (Fig. 10).

5. Interpretation with discussion

5.1. Sediment transport mechanisms

Mycielska-Dowgiałło & Ludwikowska-Kędzia (2011) developed diagrams used to interpret the depositional history of sediments (Fig. 11). Analysing the relationship between mean grain size

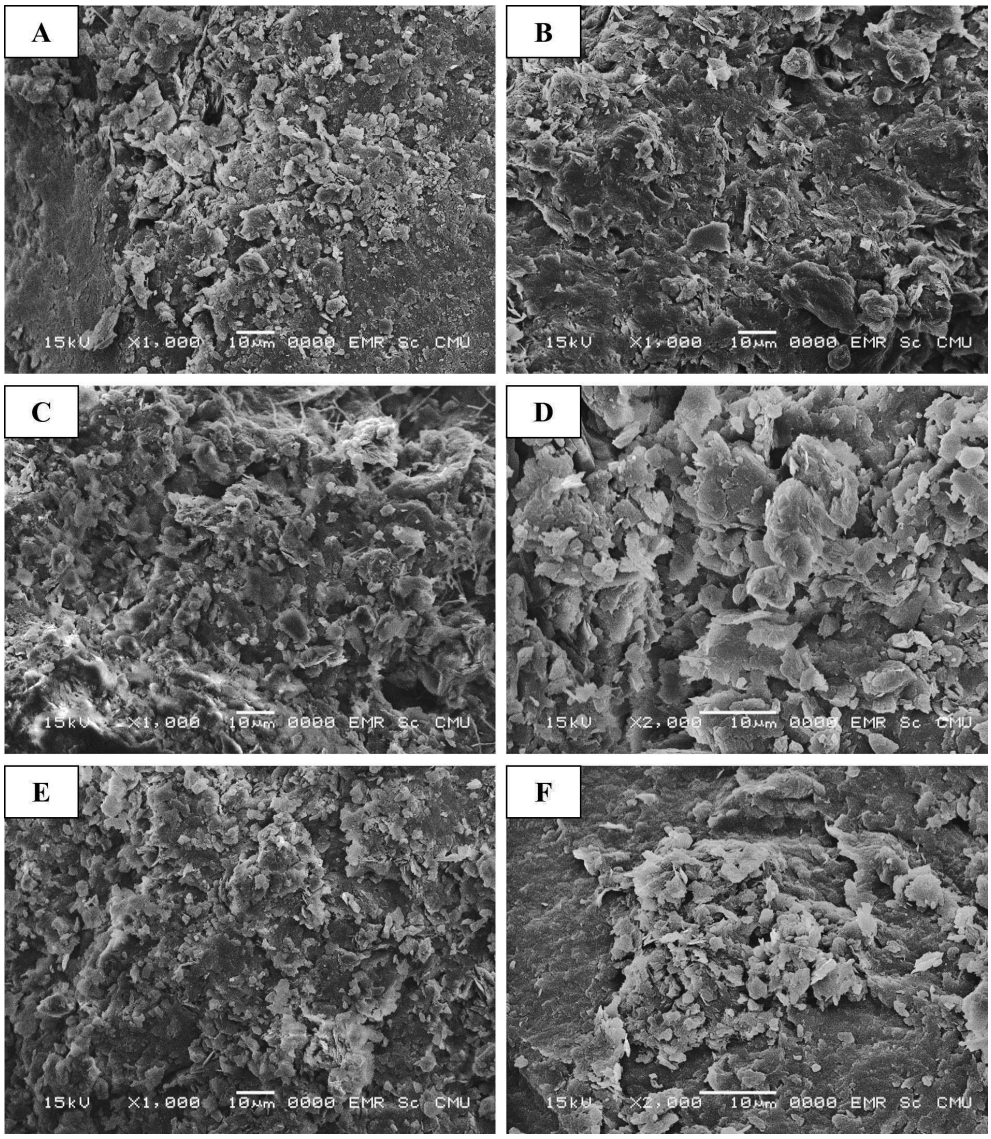

Fig. 7. Backscatter images of clay minerals from borehole A. **A –** Sample 10; **B –** Sample 20; **C –** Sample 38; **D –** Sample 66; **E –** Sample 80; **F –** Sample 99. Magnification x 1,000 (A–C, E) and x 2,000 (D, F).

and standard deviation, only sample HS16 from the Interburden Formation 1 (IF1) is plotted in the facies field of an overbank deposit, while the other samples are plotted outside this field (Fig. 11A). The plot of these two parameters (i.e., mean vs. standard deviation) is also related to the sorting. Generally, as the mean grain size increases, the sorting decreases for samples examined. Poorly sorted sediments are indicative of those deposited relatively closely to the source area. This relationship is representative of depositional environments with high variability of transport energy. Periods of low-energy transport alternate with short periods of higher-energy transport resulting in the accumulation of particularly coarse-grained material that forms poorly sorted deposits (Mycielska-Dowgiałło & Ludwikowska-Kędzia, 2011). Taking into account the palaeogeographical background, these grain-size characteristics may exclusively indicate facies formed in fluvial channels. The relationship between skewness and mean grain size shows that sample HS14 (from the parting of the seam G) is located in a field of overbank deposits (Fig. 11B). In contrast, the other samples (mostly in the lower right-hand corner), which are finer and have lower skewness, indicate stagnant water deposits or deposits filling oxbow lakes, mires (wet forest swamp or bush moor) and lacustrine depressions (Kordowski, 2003). New information is provided by the plot of standard deviation and skewness. Sample HS02 (parting of the seam H) and samples HS12, HS13 and HS23 (Inter-

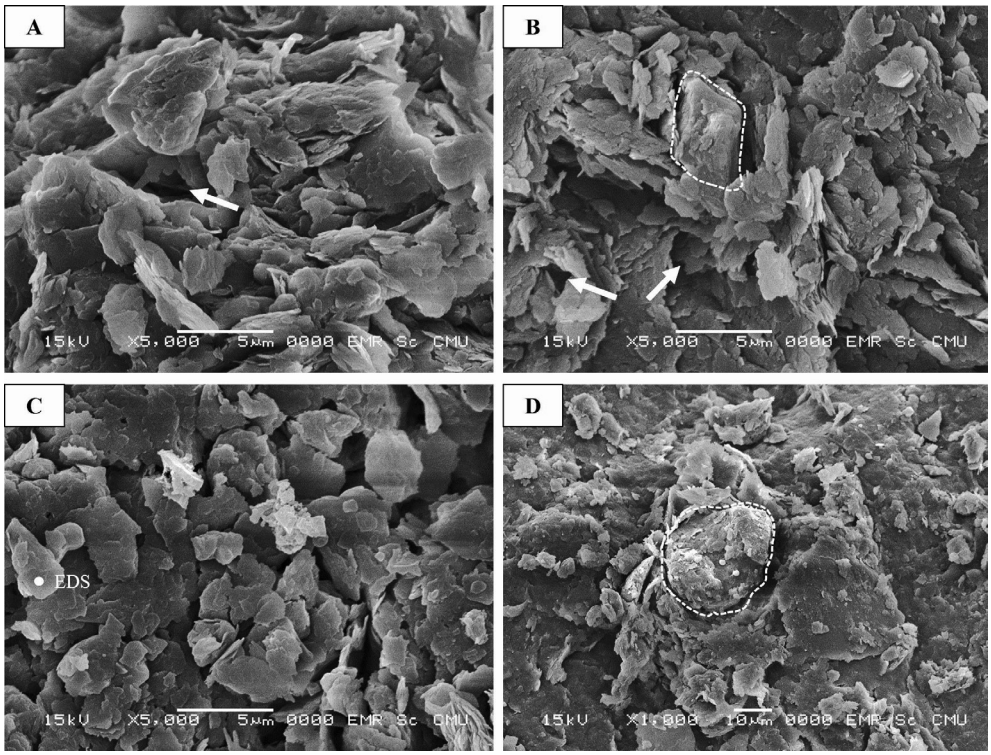

Fig. 8. Backscatter images of clay minerals from borehole A. **A –** Sample 12 shows flaky illite platelets arranged in a card-house microfabric, as indicated by the arrow; **B –** Sample 50 flaky illite platelets arranged in a card-house microfabric, as indicated by the arrow; the white dashed line shows a rhombic-shaped mineral; **C –** Sample 38 shows flake-like illite platelets oriented in a card-house microfabric, along with some grains deposited by gravity; **D –** Sample 66 shows a grain deposited by gravity (white dashed line) enclosed by flake-like illite platelets in an onion-skin arrangement, which indicates over-consolidation. Magnification x 5,000 (A–C) and x 1,000 (D).

burden Formation 1) are plotted in the domain of river channel sediments (Fig. 11C).

The proportions of sediment-size classes, together with grain-size trends that occur through several beds in the samples from borehole B, are presented together (Fig. 12). Looking at the rock units, the Underburden has a medium sand content and a very high clay content. During the deposition of the Lower Lignite Zone Formation to the Middle Lignite Zone Formation, thick lignite beds formed together with very fine-grained, organic-rich sediments. The Interburden Formation 1 represents some fluctuation of sand and a small amount of gravel within the sequence, while fine particles of silt and clay dominate this lithostratigraphical unit. The Upper Lignite Zone Formation includes a rather constant proportion of sand, silt and clay grains throughout the unit. The finer grains indicate a lower level of energy in the sedimentary accumulation process. In contrast, the coarser grains imply that the water energy required to deposit heavier and coarser grains must be higher than that required to lay down fine grains. The occurrence of several repeated cycles (sequences) of these sediments implies supply of

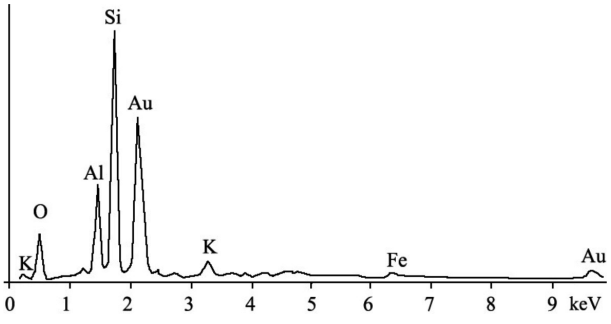

Fig. 9. Energy Dispersive X-ray Spectrum (EDS) pattern from the point in Figure 11c depicting the main elements found in the clay minerals – the presence of illite may be based on chemical composition. Note: the peak of Au is a result of coating to image a non-conductive sample at higher voltages.

siliciclastics during floods. In addition, sediment characteristics – marked by a high proportion of silt and clay, without obvious cross-stratification or imbrication in core samples – indicate that sedimentation occurred under low current strength, with a predominance of deposition from suspension (Rebesco et al., 2014).

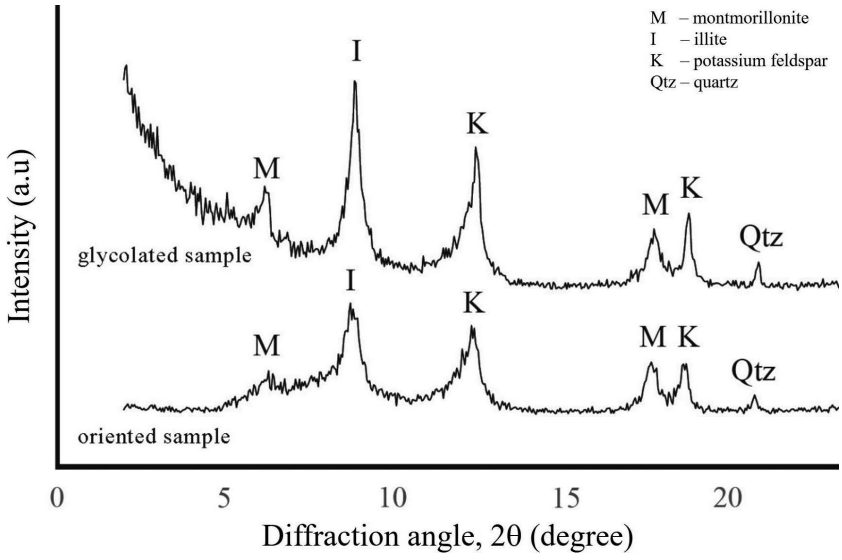

Fig. 10. Diffraction data of the clay fraction for sample 07 from borehole A. Abbreviations: montmorillonite – M, illite – I, potassium feldspar – K, and quartz – Qtz.

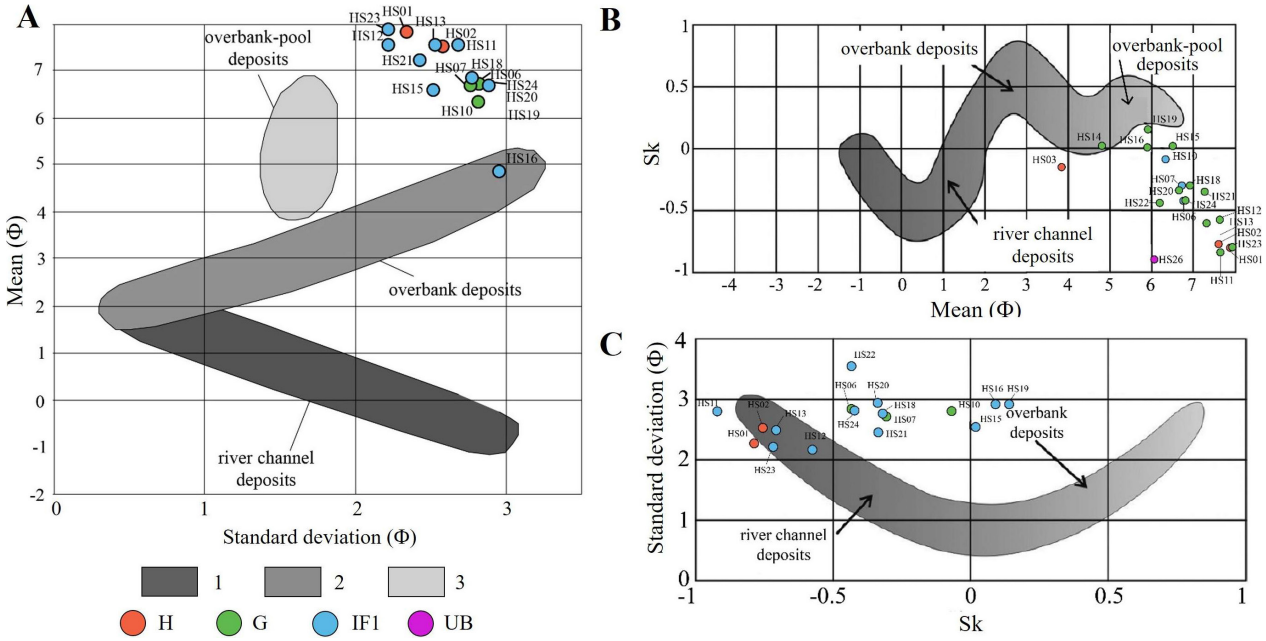

Fig. 11. Relationships of textural parameters for fine-grained siliciclastics from the lignite-bearing Hongsa Basin (modified from Mycielska-Dowgiałło & Ludwikowska-Kędzia, 2011). **A –** Mean grain diameter *vs*. standard deviation; **B –** Skewness *vs*. mean grain diameter; **C –** Standard deviation *vs*. skewness.

The log-probability curve, known as the Visher diagram, was introduced by Visher (1969) to distinguish between modes of sediment transport and hydraulic mechanisms. The three modes of transport identified are suspension, saltation and traction. The Visher plot for all sediment samples from borehole B clearly shows that suspension transport dominated over saltation and traction (Fig. 13). The log-probability curves indicate the variability in hydraulic depositional conditions for a representative sediment sample. Suspension is the primary transportation process, with traction and saltation playing secondary roles in deposition. In the Hongsa lignite deposit, the sediments were suspended mainly before being deposited. Suspension populations may range up to 95 per cent but typically fall around 70–85 per cent (see Table 3). In contrast, traction and saltation account for small amounts of poorly sorted sediments (Baiyegunhi et al., 2017).

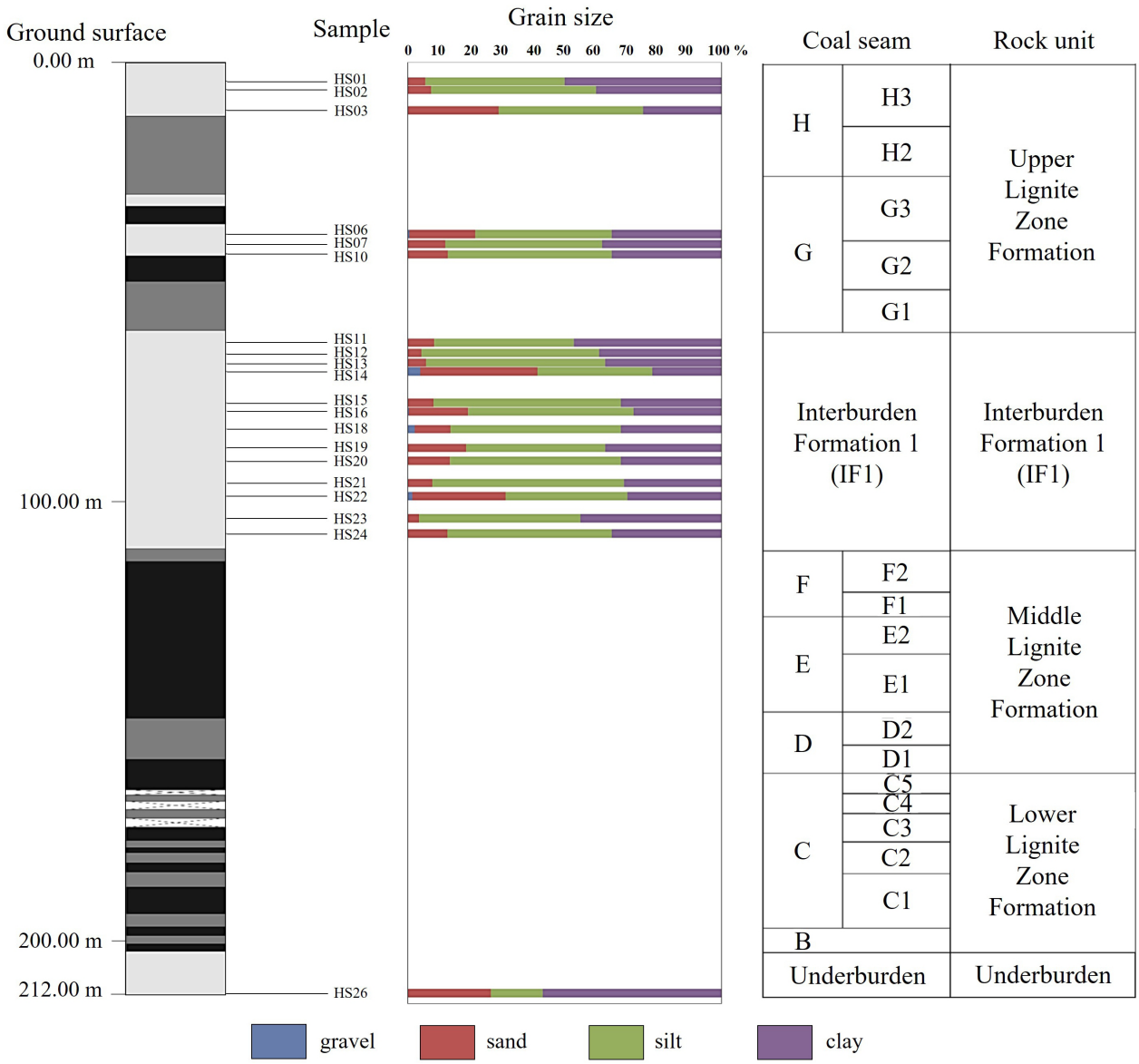

Fig. 12. Proportions of sediment size classes for fine-grained siliciclastics from the uppermost formations of borehole B, the lignite-bearing Hongsa Basin. Note the significant proportion of sand and gravel in some samples.

5.2. Clay structures, swelling clay and mitigation

Based on SEM analysis, illite platelets in the present study tend to appear in a randomly arranged card-house structure (see Figs 7, 8). The card-house structure of clays refers to an open, porous network formed during sedimentation, where clay particles, particularly those with high surface charges, such as smectites and kaolinite, stack in a disordered edge-to-face orientation. This structure typically forms in low-salinity environments where electrostatic forces between the negatively charged surfaces and positively charged edges of the clay particles lead to flocculation. The resulting arrangement increases porosity and water retention, influencing the permeability of sediments and their mechanical properties. Sediments with a card-house structure are more compressible and undergo significant volume reduction under load due to the collapse of the structure (van Olphen, 1997; Meunier, 2005; Mitchell & Soga, 2005).

In the present study, the presence of weak layers composed of a montmorillonite mixture allowed rainfall to penetrate more deeply into these slopes in comparison to homogeneous slopes (Wang et al., 2010; He et al., 2022). This is consistent with the study by Harnpa & Saenton (2017), who found that,

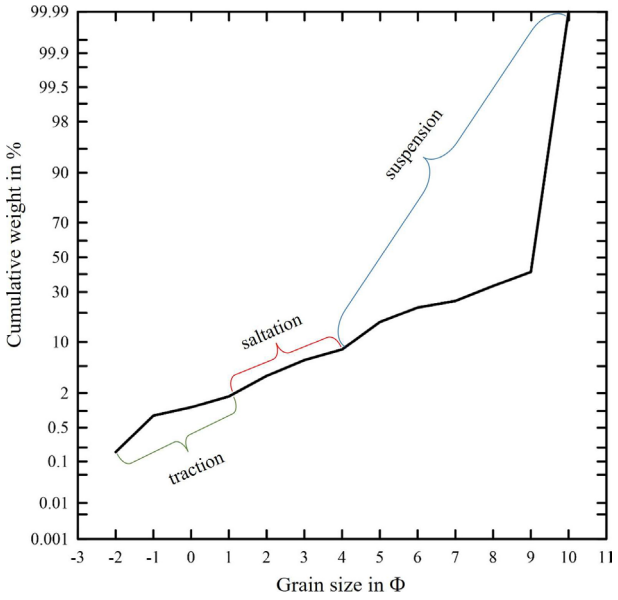

Fig. 13. The arithmetic probability curve of sample HS01 from borehole B shows the sediment transport mechanism. Note the tripartite nature of the grain-size curve.

under dry conditions, the slope of the Hongsa lignite mine pit was stable with a minimum safety factor of 1.787. However, when the pit's slope becomes saturated with water, the increased unit weight and reduced soil shear strength make the slope more prone to failure, with a minimum safety factor of 0.864 (Harnpa & Saenton, 2017).

To mitigate the effects of swelling clays, some regions use soaker hoses to water around the foundation during dry periods to help prevent foundation cracking. Adding admixtures to swelling clays can also reduce their shrink-swell properties. Additionally, implementing slope water drainage is crucial for avoiding slope failure during wet periods (Harnpa & Saenton, 2017).

5.3. Palaeoenvironmental setting of the Hongsa lignite deposit

Studies into sediment characteristics, lignite geology (Sattraburut et al., 2021b), palynology (Sattraburut et al., 2021a) and fungal spores (Sattraburut et al., 2023) have allowed the palaeoenvironment of the Hongsa Basin to be reconstructed. Therefore, the various rock units will be considered from bottom to top. The palaeoenvironmental conditions of the Hongsa Basin are summarised in Table 10.

The Underburden, which is the first zone of deposition in the basin, is composed primarily of inorganic clay-sized sediments. Its sediment composition indicates a low quartz content and a high kaolinite content, with relatively equal amounts of illite and montmorillonite. This stage of deposition can be interpreted as accumulation in stagnant water, i.e., in oxbow lakes or lakes/ponds existing on the mire (backswamp) surface (Kordowski, 2003; Widera, 2016; Chomiak et al., 2020). The grain size distribution also suggests low to very low water energy and indicates aggregation from suspension. The abundance of clay-sized sediment in this rock unit implies a lengthy duration for suspension aggregation and deposition due to the slow settling time of clay particles (Hillier, 1995). The presence of high kaolinite content suggests acidic conditions (Chaudhri & Singh, 2012), indicative of warm and humid conditions, with kaolinite being derived from the chemical weathering of feldspar or mica (Fagel et al., 2003; Dianto et al., 2019). Thus, the clay mineral assemblage infers a tropical humid climate during the Underburden deposition, which led to the weathering process.

The Lower Lignite Zone Formation is the lithostratigraphical unit in which organic-rich sediments and lignite are abundant. It is characterised by a low to medium amount of inorganic and organic-rich sediments, as well as lignite seams. Thus, the environment for deposition points to a medium amount of sediment supplied by a low-energy water flow to a wet-forest swamp or a bog (Sattraburut, 2021b). The climate at the time was subtropical to warm-temperate. From a petrographic point of view (Sattraburut, 2021b), the presence of a large number of wood fragments (xylites) – especially in seam B – indicates the formation of the mentioned lignite seams in the following types of mire: wet and dry forest swamp and bush moor (e.g., Teichmüller, 1958, 1989; Widera, 2012, 2016). Due to the high content of inorganic particles, dry forest swamps may be excluded from present considerations.

The relatively thick and high-quality lignite seams belong to the Middle Lignite Zone Formation. Inorganic sediments are scarcely found, so the environment for deposition points to a small amount of sediments delivered by a low-energy water flow to a mire environment. This may indicate that the peat accumulated in a bush moor (accumulation surface slightly above groundwater level) rather than in a wet forest swamp, where the accumulation surface is slightly below groundwater level (Teichmüller, 1958, 1989).

Inorganic sediments dominate the Interburden Formation 1 – IF1. The absence of organic-rich sediments in this unit can be interpreted as reflecting unfavourable palaeoclimatic and palaeotectonic conditions. Much of the sediments are clay, with some

Table 10. Summary table of palaeoenvironment, palaeovegetation and palaeoclimate of the Hongsa lignite deposit (modified from Sattraburut et al., 2021a).

Rock unit	Palaeoenvironment	Palaeovegetation	Palaeoclimate
Overburden	Overbank deposits, stagnant water deposits or deposits filling the oxbow lakes, mires, and lacustrine depressions	Remarkable number of conifers and temperate-like plants	Warm temperate climatic condition
Upper Lignite Zone Formation	Medium to high amounts of sediments deposited by low energy water flow to wet-forest swamp or moor bush environment	High amount of tropical to subtropical vegetation	Transition from tropical to warm temperate climatic conditions
Interburden Formation 1	Overbank deposits, stagnant water deposits or deposits filling the oxbow lakes, mires, and lacustrine depressions; several times flood	No data	High rainfall
Middle Lignite Zone Formation	Small amounts of sediments deposited by low energy water flow to a wet-forest environment	Broad-leave trees, which are Fabaceae and Apiaceae held the largest amounts of trees and herbs, respectively	Subtropical condition
Interburden Formation 2	No data	No data	No data
Lower Lignite Zone Formation	Medium amounts of sediments deposited by low energy water flow to wet-forest swamp or moor bush environment	Broad-leave trees, including *Quercus*, *Salix*, *Fagus*, *Acer*, and castanoids	Subtropical to warm-temperate conditions
Underburden	Stagnant water deposits or deposits filling the oxbow lakes, mires, and lacustrine depressions	No data	Tropical warm and humid conditions

silt and sand. This is further supported by the presence of mudstone and sandstone. Results obtained indicate that most of the samples are immature and submature, and the mud matrix content exceeds 5 per cent. This reflects a poor degree of sorting and also indicates that the sources of sediments are not far from the deposition areas. Mineralogy, based on XRD bulk compositions, shows a high abundance of quartz up to 88 per cent of the total composition. The depositional environment at the time suggests accumulation in the overbank zone, i.e., in stagnant or very slow-flowing water, poor in organic matter. The large amount of silica may be the result of leaching during heavy rainfall (Deepthy & Balakrishnan, 2005).

The possible source of the IF1 sediments is the Mesozoic bedrock bordering the Hongsa Basin in the north which consists mainly of terrigenous sandstone and siltstone with mineral assemblages similar to the ones found in the sedimentary rocks examined. Supporting evidence is the shape and size of the minerals, particularly quartz. The poor sorting and angular shape indicate a short distance of transport from an uplifted source area. The sediment supply came from several floods. The occasional floods carried suspended silt and clay from the river channels to the floodplains. As the flood waters receded, fine sediments were deposited in the distal part of the backswamp area, forming overbank deposits. It may be assumed that several floods brought also coarser sediments (sand, gravel) from sources to be deposited in the study area.

There is an alternative interpretation of the above. Simply put, the succession of fine- (clay, silt) and coarse-grained (sand, gravel) sediments can be a rock record of facies movement in the area where boreholes A and B are located. According to this hypothesis, coarse-grained sediments (e.g., as crevasse splays) were deposited in the immediate vicinity of river channels (proximal zone of the floodplain) when they were located close to the study area. In contrast, fine-grained sediments were

laid down at the same time in the distal zone of the floodplain, when the river channels, from which the mineral material came, were located far from the boreholes A and B. Such co-occurrence of sands (crevasse-splay sediments) and muds (lacustrine sediments) within lignite seams is well known, e.g., from Middle Miocene lignite deposits in central Poland (e.g., Widera, 2016; Chomiak et al., 2020; Dziamara et al., 2023; Widera et al., 2023, 2024).

The characteristics of inorganic sediments in the Upper Lignite Zone Formation are similar to those of the Interburden Formation 1, in terms of both grain size and mineral composition. This consists of abundant fine-grained sediments, indicating the same environment as the Interburden Formation 1, but with addition of organic inputs. Here, it is the presence of a high amount of montmorillonite compared to other rock units. The origin of this montmorillonite, one of the swelling clays, is different from the others. It is a product of volcanism and hydrothermal activity, and is common as an alteration product of weathered igneous and metamorphic rock minerals under alkaline conditions (Carroll, 1970). The montmorillonite in this formation (lithostratigraphical unit) may have been derived from volcanic activity in nearby areas. The Miocene-Holocene volcanic activity of the northern sector of Vietnam (Dien Bien Phu, Phu Quy and Khe Sanh) and a number of small areas in Lao PDR may be the source of erupted volcanic material. These volcanic areas include cinder cones, pyroclastic fragments and, less frequently, individual lava flows (Fedorov & Koloskov, 2005). Moreover, the presence of a small amount of gypsum reflects sulphide oxidation when sulphuric acid reacts with calcium carbonate, indicating oxidising conditions. This sulphur may also have been derived from volcanic activity.

The uppermost unit is the Overburden, which consists of both inorganic and some organic-rich sediments. In this case, the depositional environment was reconstructed based on mineral compositions and palynological assemblages. The remarkable presence of conifers and temperate-like plants indicates a warm temperate climate (Sattraburut et al., 2021a). In terms of mineral composition, the Overburden shows a fluctuating amount of quartz with a notable content of illite compared to other rock units.

Most of the inorganic sediments in the Hongsa lignite deposit consist of silt- and clay-sized particles. The characteristics of the clays studied under SEM reveal a card-house structure of illite. These particles had to be close enough to each other to interact, which led to their aggradation (Hillier, 1995). The aggregation process is attributed to salt flocculation, which occurs during the change of salinity between fine-grained particles (Hillier, 1995; Zhu et al., 2023). The rate of flocculation depends on the concentration of particles in suspension, but biological processes may also control it (Eisma, 1986). Eisma (1986) demonstrated that salt flocculation played only a minor role, while biological processes both brought and kept particles together. Many natural clay particles are coated with organic substances, mainly humic acids, which give these organic-coated clay particles a negative charge and cause flocculation. This occurs because clay particles, such as montmorillonite, illite and kaolinite, possess a negative charge in water due to isomorphic substitution, broken bonds at their edges and the dissociation of adsorbed humus (Smith, 1992; Li et al., 2021). In the Hongsa lignite deposit, electrochemical flocculation can be caused by both salts and biological processes. The suspension in freshwater enters water with different pH or salinity in a marsh (type of coastal grassy mire), and the presence of humic-coated clay particles leads to their flocculation.

Overall, the Neogene Hongsa lignite deposit consists mainly of fine-grained sediments, indicating low-energy transport currents flowing into mires (wet forest swamps and bush moors) or stagnant water (lakes, ponds, etc.). However, the presence of sand and gravel indicates high-energy flood events that brought coarser grains into the depositional area – backswamp. The poor sorting and angular shapes of the grains reflect the close proximity of sources. The mineral assemblages indicate that the sediments are recycled components derived from sedimentary rocks exposed along the northern border of the Hongsa Basin. Another explanation for the presence of fine- and coarse-grained sediments in the studied sections (i.e., boreholes A and B) may be the location of the study area relative to the river channels. The above-mentioned sediments could have been deposited in the distal or proximal zone of the overbank (backswamp) area, respectively. Finally, based on palynological analysis, the depositional age of the Hongsa Basin ranged from the Middle to Late Miocene (Sattraburut et al., 2021a, 2023).

5.4. Possible sources of sediments in the Hongsa lignite deposit

The basement of the Hongsa Basin is composed of red terrigenous rocks of the late Mesozoic age (Salyapongse et al., 2000; Hofmann et al., 2008),

correlatable with the Sao Khua Formation of the Khorat Group, which is considered to be of Early Cretaceous age (Department of Mineral Resources, 2007). These rocks consist mainly of reddish-brown siltstones, sandstones and conglomerates, indicating a predominantly fluvial depositional environment under semi-arid to arid climatic conditions (Racey et al., 1996; Buffetaut et al., 2005; Rattana, 2020; Shen & Siritongkham, 2020; Manitkoon et al., 2022). These Mesozoic rocks may be the source of both sediments and reworked palynomorphs and sediments.

The Hongsa Basin developed as a result of a major tectonic event in southeast Asia, involving interaction of the Indian and Eurasian plates. Cenozoic clockwise rotation of crustal blocks has been observed in mainland southeast Asia (Metcalfe, 2017). This led to the leftward movement of crustal blocks, resulting in the development of transtensional basins, known as pull-apart basins, in this region (Schneider & Göthel, 2001). The formation of the Hongsa Basin was influenced by the Northern Thailand Fault Zone. During its tectonic activity, erosion from the uplifted rocks led to the transport of sediments and sporomorphs from the Mesozoic bedrock into the basin. Plate tectonics was a major control on rapid erosion, more than the heavy rainfall in southern Indo-China. On the other hand, rainfall drives moderate erosion in areas that are tectonically inactive (Clift et al., 2006).

6. Conclusions

Neogene organic-rich sediments from the Hongsa lignite deposit in northwestern Lao PDR (Laos) were analysed for sedimentary characteristics, demonstrating that this lignite deposit consists primarily of fine-grained sediments, mostly clay and silt, indicating a low-energy environment. The presence of thick fine-grained sediments indicates a long period of relatively stable conditions in Hongsa tectonism, possibly in a waterlogged and/or mire (wet forest swamp and bush moor) environment.

In terms of mineral composition, quartz is the major component, followed by illite and kaolinite. Some layers also contain small amounts of montmorillonite and gypsum. In addition, the characteristics of the clays, observed by SEM, reveal a card-house structure of illite. This reflects the settling of particles from suspension due to electrochemical flocculation, potentially influenced by both salts and biological processes. Most likely, the flocculation process occurred when freshwater of varying pH levels entered the salty coastal mire (marsh), leading to the merging of humic-coated clay particles into larger aggregates.

Acknowledgements

The authors extend their thanks to Hongsa Power Co. Ltd. for granting permission and facilitating access to the information, data and core samples from the Hongsa Coal Mine used in the present study, and also acknowledge the Department of Geological Sciences, Faculty of Science, Chiang Mai University, Thailand, for technical support in the laboratory work. Last but not least, the authors appreciate the anonymous reviewers for their meticulous reviews of the original typescript and valuable comments and suggestions.

References

Aitchison J.C., Ali J.R. & Davis A.M., 2007. When and where did India and Asia collide? *Journal of Geophysical Research* 112, B05423.

ASTM International, 2008. *Standard test method for particle-size analysis of soils (ASTM D 422-63)*. [In:] Annual book of ASTM standards (vol. 04.08, pp. 10–17). West Conshohocken, USA.

Baiyegunhi C., Liu K. & Gwavava O., 2017. Grain size statistics and depositional pattern of the Ecca Group sandstones, Karoo Supergroup in the Eastern Cape Province, South Africa. *Open Geosciences* 9, 554–576.

Bennett R.H., Bryant W.R., Hulbert M.H., Chiou W.A., Faas R.W., Kasprowicz J., Li H., Lomenick T., O'Brien N.R., Pamukcu S., Smart P., Weaver C.E. & Yamamoto T., 1991. *Microstructure of Fine-Grained Sediments*. Springer-Verlag, New York, 572 pp.

Blott S.J. & Pye K., 2001. Gradistat: A grain size distribution and statistics package for the analysis of unconsolidated sediments. *Earth Surface Processes and Landforms* 26, 1237–1248.

Brindley G.W. & Brown G., 1980. *Crystal structures of clay minerals and their X-ray Identification*. Mineralogical Society of Great Britain and Ireland, London, 495 pp.

Buffetaut E., Suteethorn V., Loeuff J.L., Khansubha S., Tong H. & Wongko K., 2005. *The Dinosaur fauna from the Khok Kruat Formation (Early Cretaceous) of Thailand*. International Conference on Geology, Geotechnology and Mineral Resources of Indochina, Khon Kaen, Thailand, 575–581.

Burri P., 1989. *Hydrocarbon potential of Tertiary intermontane basins in Thailand*. [In:] T. Thanasuthipitak & P. Ounchanum (Eds): International symposium on intermontane basins: Geology & resources, Chiang Mai, Thailand, 3–12.

Carroll D., 1970. *Clay Minerals: A Guide to Their X-ray Identification*. The Geological Society of America, California, 80 pp.

Chamley H., 1989. *Clay Sedimentology*. Springer-Verlag, Berlin Heidelberg, 623 pp.

Chaodumrong P. & Songtham W., 2014. *Tectonic evolution and paleogeographic history*. [In:] Geology of Thailand. Ministry of Natural Resources and Environment, Bangkok, Thailand, 263–287.

Chaudhri A.R. & Singh M., 2012. Clay minerals as climate change indicators – A case study. *American Journal of Climate Change* 1, 231–239.

Chomiak L., Urbański P. & Widera M., 2020. Architektura i geneza iłów w górnym poziomie węgli brunatnych formacji poznańskiej (środkowy miocen) – odkrywka Tomisławice koło Konina w środkowej Polsce [Architecture and origin of clays within the upper part of lignites of the Poznań Formation (Middle Miocene) – the Tomisławice lignite opencast mine near Konin, central Poland]. *Przegląd Geologiczny* 68, 526–534.

Clift P.D., Carter A., Campbell I.H., Lap N.V., Allen C.M. & Tan M.T., 2006. Thermochronology of mineral grains in the Red and Mekong Rivers, Vietnam: Provenance and exhumation implications for Southeast Asia. *Geochemistry Geophysics Geosystems* 7, 1–28.

Deepthy R. & Balakrishnan S., 2005. Climatic control on clay mineral formation: Evidence from weathering profiles developed on either side of the Western Ghats. *Journal of Earth System Science* 114, 545–556.

Department of Mineral Resources, 2007. *Geological map of Nan Province*. Department of Mineral Resources, Bangkok (in Thai).

Dianto A., Subehi L., Ridwansyah I. & Hantoro W.S., 2019. Clay minerals in the sediments as useful paleoclimate proxy: Lake Sentarum case study, West Kalimantan, Indonesia. *IOP Conference Series: Earth and Environmental Science* 311, 012036.

Dziamara M., Kaczmarek P., Klęsk J., Wachocki R. & Widera M., 2023. Facies and statistical analyses of a crevasse-splay complex at the Tomisławice opencast lignite mine in central Poland. *Geologos* 29, 173–181.

Eisma D., 1986. Flocculation and deflocculation of suspended matter in estuaries. *Netherlands Journal of Sea Research* 20, 183–199.

Fagel N., Boski T., Likhoshway L. & Oberhaensli H., 2003. Late Quaternary clay mineral record in Central Lake Baikal (Academician Ridge, Siberia). *Palaeogeography, Palaeoclimatology, Palaeoecology* 193, 159–179.

Fedorov P. & Koloskov A.V., 2005. Cenozoic Volcanism of Southeast Asia. *Petrology* 13, 352–380.

Folk R.L., 1980. *Petrology of sedimentary rocks*. Hemphill Publishing Company, Austin, 182 pp.

Folk R.L. & Ward W.C., 1957. Brazos River bar: A study in the significance of grain size parameters. *Journal of Sedimentary Research* 27, 3–26.

Foster M.D., 1954. The relation between composition and swelling in clays. *Clays and Clay minerals* 3, 205–220.

Friederich M.C., Moore T.A. & Flores R.M., 2016. A regional review and new insights into SE Asia Cenozoic coal-bearing sediments: Why does Indochina have such extensive coal deposits? *International Journal of Coal Geology* 166, 2–35.

Hall R. & Morley C.K., 2004. *Sundaland basins*. [In]: P. Clift, W. Kuhnt & D.E. Hayes (Eds): Continent-ocean Interactions Within the East Asian Marginal Seas. American Geophysical Union, Washington DC, 55–85.

Harnpa T. & Saenton S., 2017. *Stability analysis of Hongsa Coal Mine's pit walls, Xaignabouli Province, Laos PDR*. The National and International Graduate Research Conference, Khon Kaen, Thailand, 89–95.

He L., Qiu J., Hu Q., Wang H., Feng S., Gu Y. & Zeng J., 2022. Micro-mechanism of shear strength and water stability enhancement of montmorillonite by microwave heating. *Materials Research* 25, e20210260.

Hillier S., 1995. *Erosion, sedimentation and sedimentary origin of clays*. [In:] B. Velde (Ed.): Origin and mineralogy of clays: Clays and the environment. Springer-Verlag, Berlin, 162–219.

Hofmann L., Blunck S., Dittrich W., Kraemer T., von Schwarzenberg T. & Wall G., 2008. *Mine master plan for the Hongsa Mine Mouth Power Project, Lao P.D.R.: Final Report*. RWE Power International, Koeln.

Hongsa Power, 2024. *Hongsa Power Company Limited (HPC)*. Available at https://www.hongsapower.com/index.php?model=cms&view=item&layout=page&id=1

Jackson M.L., 2018. Soil chemical analysis: Advanced course (2nd ed.). University of Wisconsin, Madison, 930 pp.

Jain A.K., 2014. When did India-Asia collide and make the Himalya? *Current Science* 106, 2–25.

Kordowski J., 2003. Struktury wewnętrzne i uziarnienie osadów pozakorytowych doliny dolnej Wisły w Kotlinie Toruńskiej i Basenie Unisławskim [Structures and granulometry of overbank deposits of the lower Vistula River valley in the Toruń and Unisław Basins]. *Przegląd Geograficzny* 75, 601–621.

Kumar P.A. & Patterson J., 2008. Granulometric study of Tharuvaikulam and Thirespuram, Gulf of Mannar, southeast coast of India. *Journal of the Marine Biological Association of India* 50, 127–133.

Lacassin R., Maluski H., Leloup P.H., Tapponnier P., Hinthong C., Siribhakdi K., Chuaviroj S. & Charoenravat A., 1997. Tertiary diachronic extrusion and deformation of western Indochina: Structural and 40Ar/39Ar evidence from NW Thailand. *Journal of Geophysical Research* 102 (B5), 10013–10037.

Li X., Gu H., Huang A. & Fu L., 2021. Bonding mechanism and performance of rectorite/ball clay bonded unfired high alumina bricks. *Ceramics International* 47, 10749–10763.

Manitkoon S., Deesri U., Lauprasert K., Warapeang P., Nonsrirach T., Nilpanapan A., Wongko K. & Chanthasit P., 2022. Fossil assemblage from the Khok Pha Suam locality of northeastern, Thailand: an overview of vertebrate diversity from the Early Cretaceous Khok Kruat Formation (Aptian-Albian). *Fossil Record* 25, 83–98.

Metcalfe I., 2017. Tectonic evolution of Sundaland. *Bulletin of the Geological Society of Malaysia* 63, 27–60.

Meunier A., 2005. *Clays*. Spinger, Berlin, 472 pp.

Mitchell J. K. & Soga K., 2005. Fundamentals of soil behavior (3rd ed.). John Wiley & Sons, Hoboken, 592 pp.

Moore D.M. & Reynolds R.C., 1997. *X-ray diffraction and the identification and analysis of clay minerals* (2nd ed.). Oxford University Press, Oxford, 400 pp.

Morley C.K. & Racey A., 2011. *Tertiary stratigraphy*. [In:] M.F. Ridd, A.J. Barber & M.J. Crow (Eds): The geology of Thailand. The Geological Society of London, London, 223–271.

Mycielska-Dowgiałło E. & Ludwikowska-Kędzia M., 2011. Alternative interpretations of grain-size data from Quaternary deposits. *Geologos* 17, 189–203.

NASA/METI/AIST/Japan Spacesystems & U.S./Japan ASTER Science Team., 2018. ASTGTM v003 ASTER Global Digital Elevation Model 1 arc second. Available at https://doi.org/10.5067/ASTER/ASTGTM.003

Phouthonesy P., 2021. *The Lao PDR Country Report*. [In:] P. Han & S. Kimura (Eds): Energy Outlook and Energy Saving Potential in East Asia 2020. ERIA, Jakarta, 213–238.

Phusuwan S., Xayalath S. & Pongpa-ngan L., 2015. *Challenging Hongsa resettlement and livelihoods: The first mine-mouth power plant project in Lao PDR*. Proceeding of 35th Annual Conference of the International Association for Impact Assessment, Florence, Italy, 1–5.

Piman T. & Manish S., 2017. *Case study on sediment in the Mekong River basin: Current state and future trends. Project Report 2017-03*. Stockholm Environment Institute, Stockholm, 45 pp.

Racey A., Love M.A., Canham A.C., Goodall J.G.S., Polachan S. & Jones P.D., 1996. Stratigraphy and reservoir potential of the Mesozoic Khorat Group, NE Thailand. Part 1: Stratigraphy and sedimentary evolution. *Journal of Petroleum Geology* 19, 5–40.

Ratanasthien B., 1975. *The geochemistry of some recent argillaceous sediment*. The University of Aston in Birmingham, 348 pp.

Rattana P., 2020. *Stratigraphy and geochemistry of rock salt from Maha Sarakham formation in Changwat Chaiyaphum, northeastern Thailand*. Chulalongkorn University Theses and Dissertations, Bangkok, 356 pp.

Rebesco M., Hernández-Molina F.J., Rooij D.V. & Wåhlin A., 2014. Contourites and associated sediments controlled by deep-water circulation processes: State-of-the-art and future considerations. *Marine Geology* 352, 111–154.

Salyapongse S., Fontaine H. & Sashida K., 2000. *Petrologic and paleontologic constraints on age of rock associations – pyroclastics, volcaniclastics and limestones in Nan, Phayao and Prae Provinces (research report)*. Department of Mineral Resources. Bangkok, Thailand, 137–170.

Sattraburut T., Ratanasthien B. & Thasod S., 2021a. Palaeovegetation and palaeoclimate of Tertiary sediments from Hongsa Coalfield, Xayabouly Province, Lao PDR – Implication from palynofloras. *Songklanakarin Journal of Science and Technology* 43, 648–659.

Sattraburut T., Thasod Y., Ratanasthien B. & Kandharosa W., 2021b. Petrographic and chemical characterizations of coals from Hongsa coal mine, Xayabouly Province, Lao PDR. *Suranaree Journal of Science and Technology* 28, 030037.

Sattraburut T., Ratanasthien R. & Thasod Y., 2023. Fungal spores from Neogene sediments of the Hongsa Basin, Lao PDR. *Tropical Natural History* 23, 82–96.

Sattraburut T., Thasod Y. & Ratanasthien B., 2017. *Maceral association in coal-bearing formations of Hongsa coal deposits, Northwestern Lao PDR*. The 6th International Graduate Research Conference, Chiang Mai, Thailand.

Schneider W. & Göthel M., 2001. Geology and petrography of Young Tertiary lignite seams in the Hongsa Basin (Laos, Indochina). *Geologica Saxonica* 46/47, 149–167.

Shen L. & Siritongkham N., 2020. The characteristics, formation and exploration progress of the potash deposits on the Khorat Plateau, Thailand and Laos, Southeast Asia. *China Geology* 3, 67–82.

Shrestha B., Maskey S., Babel M.S., van Griensven A. & Uhlenbrook S., 2018. Sediment related impacts of climate change and reservoir development in the Lower Mekong River Basin: a case study of the Nam Ou Basin, Lao PDR. *Climatic Change* 149, 13–27.

Tapponier P., Peltzer G. & Armijo R., 1986. On the mechanics of the collision between India and Asia. *Geological Society, London, Special Publications* 19, 113–157.

Teichmüller M., 1958. Rekonstruktion verschiedener Moortypen des Hauptflözes der Niederrheinischen Braunkohle [Reconstruction of various peat types of the main seam of the Lower Rhine lignite]. *Fortschritte in der Geologie von Rheinland und Westfalen* 2, 599–612.

Teichmüller M., 1989. The genesis of coal from the viewpoint of coal petrology. *International Journal of Coal Geology* 12, 1–87.

Thasod Y., Ratanasthien B., Tanaka S., Saegusa H. & Nakaya H., 2007. Fine-fraction clays from Chiang Muan Mine, Phayao Province, Northern Thailand. *Science Asia* 33, 13–21.

van Olphen H., 1977. *An introduction to clay colloid chemistry: For clay technologists, geologists, and soil scientists (2nd ed.)*. John Wiley, New York, 318 pp.

Vilaihongs M. & Areesiri S., 1997. Geology of lignite deposit and tectonic evolutions in Hongsa Tertiary basin, Khwaeng Xayabouly northern Lao PDR. [In:] Dheeradilok P., Hinthong C., Chaodumrong P., Putthapiban P., Tanasathien W., Utha-aroon C., Sattayarak N., Nuchanong T., Techawan S. (Ed): Proceeding of the International Conference on Stratigraphy and Tectonic Evolution of Southeast Asia and the South Pacific, Bangkok, Thailand.

Virk H.S., 2015. *Nanomaterials: Basic concepts and applications*. Trans Tech Publications Ltd., Bäch, Switzerland, 212 pp.

Visher G.S., 1969. Grain size distributions and depositional processes. *Journal of Sedimentary Petrology* 39, 1074–1106.

Wang R., Zhang G. & Zhang J-M., 2010. Centrifuge modelling of clay slope with montmorillonite weak layer under rainfall conditions. *Applied Clay Science* 50, 386–394.

Welton J.E., 2003. *SEM petrology atlas – Methods in exploration series No. 4*. The American Association of Petroleum Geologists. Oklahoma, USA.

Widera M., 2012. Macroscopic lithotype characterisation of the 1st Middle-Polish (1st Lusatian) Lignite Seam in the Miocene of central Poland. *Geologos* 18, 1–11.

Widera M., 2016. Depositional environments of overbank sedimentation in the lignite-bearing Grey Clays Mem-

ber: New evidence from Middle Miocene deposits of central Poland. *Sedimentary Geology* 335, 150–165.

Widera M., Chomiak L. & Wachocki R., 2023. Distinct types of crevasse splays formed in the area of Middle Miocene mires, central Poland: Insights from geological mapping and facies analysis. *Sedimentary Geology* 443, 106300.

Widera M., Dziamara M., Klęsk J. & Wachocki R., 2024. Four in one: a new crevasse-splay complex in the middle Miocene of central Poland. *Annales Societatis Geologorum Poloniae* 94, 1–18.

Zhu H., Li S., Hu Z., Ju Y., Pan Y., Yang M., Lu Y., Wei M. & Qian W., 2023. Microstructural observations of clay-hosted pores in black shales: implications for porosity preservation and petrophysical variability. *Clay Minerals* 58, 310–323.

Manuscript submitted: 26 August 2024
Revision accepted: 15 October 2024